Title :

ORCHIDEE MICT-LEAK (r5459), a global model for the production, transport and transformation of dissolved organic carbon from Arctic permafrost regions, Part 2: Model evaluation over the Lena River basin.

Authors:

S.P.K. Bowring[1], R. Lauerwald[2], B. Guenet[1], D. Zhu[1], M. Guimberteau[1,3], P. Regnier[2], A. Tootchi[3], A. Ducharne[3], P. Ciais[1]

Affiliations:

[1] Laboratoire des Sciences du Climat et de l'Environnement, LSCE, CEA, CNRS, UVSQ, 91191 Gif Sur Yvette, France

[2] Department of Geoscience, Environment & Society, Université Libre de Bruxelles, Bruxelles, Belgium

[3] Sorbonne Université, CNRS, EPHE, Milieux environnementaux, transferts et interaction dans les hydrosystèmes et les sols, Metis, 75005 Paris, France

Abstract

In this second part of a two-part study, we perform a simulation of the carbon and water budget of the Lena catchment with the land surface model ORCHIDEE MICT-LEAK, enabled to simulate dissolved organic carbon (DOC) production in soils and its transport and fate in high latitudes inland waters. The model results are evaluated in their ability to reproduce the fluxes of DOC and carbon dioxide (CO_2) along the soil-inland water continuum, and the exchange of CO_2 with the atmosphere, including the evasion outgassing of CO_2 from inland waters. We present simulation results over years 1901-2007, and show that the model is able to broadly reproduce observed state variables and their emergent properties across a range of interacting physical and biogeochemical processes, including: 1) Net primary production (NPP), respiration and riverine hydrologic amplitude, seasonality and inter-annual variation; 2) DOC concentrations, bulk annual flow and their volumetric attribution at the sub-catchment level; 3) High headwater versus downstream CO_2 evasion, an emergent phenomenon consistent with observations over a spectrum of high latitude observational studies. (4) These quantities obey emergent relationships with environmental variables like air temperature and topographic slope that have been described in the literature. This gives us confidence in reporting the following additional findings: Of the ~34TgC yr^{-1} left over as input to soil matter after NPP is diminished by heterotrophic respiration, 7 TgC yr^{-1} is leached and transported into the aquatic system. Of this, over half (3.6 TgC yr^{-1}) is evaded from the inland water surface back into the atmosphere and the remainder (3.4 TgC yr^{-1}) flushed out into the Arctic Ocean, mirroring empirically derived studies. These riverine DOC exports represent ~1.5% of NPP. DOC exported from the floodplains is dominantly sourced from recent, more 'labile' terrestrial production, in contrast to DOC leached from the rest of the watershed with runoff and drainage, which is mostly sourced from recalcitrant soil and litter. All else equal, both historical climate change (a spring/summer warming of 1.8°C over the catchment) and rising atmospheric CO_2 (+85.6ppm) are diagnosed from factorial simulations to contribute similar, significant increases in DOC transport via primary production, although this similarity may not hold in the future.

1 Introduction

A new branch of the high latitude-specific land surface component of the IPSL Earth System model, ORCHIDEE MICT-LEAK (r5459), was enabled to simulate new model processes of soil dissolved organic carbon (DOC) and CO_2 production, and their advective/diffusive vertical transport within a discretized soil column as well as their transport and transformation within the inland water network, in addition to improved representation of hydrological and carbon processes in floodplains. These additions, processes first coded in the model ORCHILEAK (Lauerwald et al., 2017) and implemented within the high latitude base model ORCHIDEE-MICT v8.4.1 (Guimberteau et al., 2018), were described in detail in Part 1 of this study. In essence, plant litter and soil carbon are transformed by microbial degradation to DOC and CO2; the DOC is itself either respired to CO2 or adsorbed, or transformed to particulate soil carbon. DOC can then be transferred by precipitation-dependent water flow laterally across the terrestrial landmass, in surface or subsurface flows to streams and rivers, whereupon it may either be respired within the water column or exported to the marine realm. A flow diagram depicting these flows and the residence times of the respective carbon pools, reproduced from Part 1 of this study, is given in Figure S1a,b. This second part of our study deals with the validation and application of our model. We validate simulation outputs against observation for present-day and run transient simulations over the historial period (1901-2007) using the Lena River basin as test case. The simulation setup and rationale for choice of simulation basin are outlined below.

2 Simulation Rationale

The Lena river basin, which is bounded by the region 52-72°N; 102-142°E, was chosen as the basin for model evaluation because it is the largest DOC discharge contribution amongst the Arctic rivers, according to some estimates (Raymond et al., 2007; Holmes et al., 2012), with its 2.5 million km^2 area (befitting our coarse-grid resolution) discharging almost 20% of the summed discharge of the largest six Arctic rivers, its large areal coverage by Podzols (DeLuca and Boisvenue, 2012), and the dominance of DOC versus particulate organic carbon (POC) with 3-6Tg DOC-C yr^{-1} vs. 0.03-0.04 Tg POC-C yr^{-1} (Semiletov et al., 2011) in the total OC discharge load –factors all broadly representative of the Eurasian Arctic rivers. Compared to other Eurasian rivers, the Lena is relatively well studied, which provides data across the range of soil, hydrologic, geochemical and ecological domains over space and time, that enable us to perform adequate model evaluation.

Climatological forcing is input from the Global Soil Wetness Project Phase 3 (GSWP3) v.0 data, based on 20th Century reanalysis using the NCEP land-atmosphere model and downscaled to a 0.5°, 3-hourly resolution covering the period 1901 to 2007 (Supplement, Table S1). This is then upscaled to 1° resolution and interpolated to a 30 minute timestep to comply with the timestep of ORCHIDEE's surface water and energy balance calculation period. Precipitation was partitioned into rainfall and snowfall, and a correction for wind-induced undercatch was also applied. These are described in greater detail in Guimberteau et al. (2018). Over the simulation period under this climatological forcing dataset, the Lena basin experiences a mean thaw period warming of 1.8°C, while atmospheric CO_2 concentrations increase by 85.6ppm. The GSWP3 dataset was chosen for its prior suitability as input its relative performance in

simulating the interannual variability and seasonality of Pan-Arctic riverine discharge in ORCHIDEE-MICT (Guimberteau et al., 2018), as compared to another data-driven climate forcing product, CRUNCEP v7 (Kalnay et al., 1996; New et al., 1999).. Indeed, under CRUNCEP v7, ORCHIDEE-MICT was shown to underestimate river discharge by as much as 83% over the Yukon basin. An improved floodplains area input file for the Lena basin (Tootchi et al., 2019) was used to drive the simulation of floodplain dynamics (Supplement, Table S1). The model structure is described in Part 1 of this study, however we describe how the fluxes are generated with respect to the results obtained by this study in some detail in the initial description of the results, below (Section 4.1).

3 Simulation Setup

As detailed in Part 1 (Section 3.1) of this study, the soil carbon stock used by our model was reconstituted from a 20,000 year soil carbon spinup of an ORCHIDEE-MICT run from Guimberteau et al. (2018) and run to quasi-steady state equilibrium for the Active and Slow carbon pools (Supplement, Fig. S1b) under the new soil carbon scheme used in the model configuration of the present study (Fig. 1). After some adjustment runs to account for different data read/write norms between ORCHIDEE-MICT and this model version, the model was then run in transient mode under historical climate, land cover and atmospheric CO_2 concentrations. A summary of the step-wise procedure for simulation setup described above is detailed graphically in Fig. 1. Simulations were run over the Lena river basin (Fig. 3a) for the climate, CO_2 and vegetation input forcing data (Supplement, Table S1) over 1901-2007 at a 1 degree resolution (Fig. 1), to evaluate the simulated output of relevant carbon fluxes and hydrologic variables against their observed values, as well as those of emergent phenomena arising from their interplay (Fig. 1). We evaluate at the basin scale because the isolation of a single geographic unit allows for a more refined analysis of simulated variables than doing the same over the global Pan-Arctic, much of which remains poorly accounted for in empirical databases and literature. The literature studies used in this evaluation are summarised in Table S2.

In order to derive an understanding of the environmental drivers of carbon cycling in the Lena watershed and analyse the model sensitivity to the corresponding forcing data, alternative simulations were run with constant climate and CO_2 conditions (Table 1, and Supplement Table S1). Thus a factorial simulation was devised, consisting of 2 factors and 3 simulations whose inputs were otherwise identical but for the investigated factor (Table 1).

4 Results and Interpretation

We refer to different simulations performed in this study according to the sensitivity factors to which they are subjected. The transient, historical climate and atmospheric CO_2 -forced simulations are hereafter referred to as the "Control" (CTRL) scenario, for ease of interpretation . The "CLIM" and "CO_2" scenarios are those simulations for which climate variability and atmospheric CO_2 were held constant at their pre-industrial levels, respectively (Table 1). The following evaluation sections compare observations solely against the CTRL. The subsequent section will evaluate this comparison against the factorial simulations described above.

The overall carbon budgets and their fluxes as generated by each of the simulations are shown in Figs. 2 and 11 and discussed in detail at the end of the evaluation. Below, we examine that budget's component parts, in the following sequential order: In section 4.1 we briefly look through the overall carbon budget of the entire basin, discussing component fluxes of the budget, their values and what they mean. Section 4.2 evaluates DOC discharge, followed by DOC concentrations in export (4.3), dissolved CO_2 transport in rivers and its evasion from the river surface (4.4), emergent phenomena with respect to CO_2 evasion compared to river size (4.5.1) and DOC concentrations and slope (4.5.2), followed by DOC reactivity pools (4.6). NPP and soil respiration rates, evaluated at the Pan-Arctic scale for ORCHIDEE-MICT in Guimberteau et al. (2018), are evaluated for the Lena basin in the Supplement (Text S2). Wherever possible, model output are compared with available in situ observations, while emergent relationships between fluxes or concentrations and environmental controls found in observatons are also drawn from the model output, to provide a 'process oriented' evaluation of the model. In Section 4.7 we discuss the overall drivers of the fluxes simulated by our model with respect to the two CLIM and CO_2 factorial simulations and the implications of these for the future.

4.1 Model Output: Carbon Budget

Fig. 2 summarises the simulated components of the carbon (C) cycle across the Lena basin, averaged over the decade 1998-2007. C inputs to terrestrial ecosystems are dominated by photosynthetic input (GPP). GPP assimilates (875 TgC yr^{-1}) are either used as metabolic substrate by plants and lost as CO_2 by plant respiration processes (376 TgC yr^{-1}) or soil respiration processes (465 TgC yr^{-1}), leaving behind annual growth in terrestrial C storage (net biome productivity (NBP)), an atmospheric CO_2 sink of 34 TgC yr^{-1}. Further C inputs are delivered to the terrestrial surface via a combination of atmospheric deposition, rainwater dissolved C, and the leaching of canopy C compounds. These sum to a flux transported to the soil surface (4.6 TgC yr^{-1}) by throughfall (see Part 1, Section 2.5).

In the soil, DOC is produced by the decomposition of litter and soil organic carbon (SOC) pools (see Part 1, Section 2.4 and Fig. 2) and can be ad- or de- sorbed to solid particles (see Part 1 of this study, Section 2.11), while there is a continuous exchange of DOC with (solid) soil organic carbon. The interplay between decomposition and sorption leads to DOC concentration changes in the soil solution. DOC in the soil solution as well as a fraction of dissolved CO_2 produced in the root zone from root and microbial respiration is exported to rivers along the model's two hydrological export vectors, surface runoff and deep drainage (Part 1, Section 2.6). For the Lena basin simulations, these fluxes of C exported from soils amount to 5.1 and 0.2 TgC yr^{-1}, for DOC and CO_2 respectively. Three water pools, representing streams, rivers and groundwater and each containing dissolved CO_2 and well as DOC of different reactivity, are routed through the landscape and between grid cells following the river network in the catchment (Part 1, Section 2.7). In addition, seasonally flooded soils located in low, flat grid cells next to the river network (see Part 1, Section 2.8) export DOC (0.57 TgC yr^{-1}) and CO_2 (1.54 TgC yr^{-1}) to the river network when their inundation occurs. Part of this leached inundated material is re-infiltrated back into the soil from the water column during floodplain recession ('Return' flux, 0.45 TgC yr^{-1}). During its transport through inland waters, DOC can be decomposed into CO_2 (2.1 TgC yr^{-1}) and a fraction of river CO_2 produced from

DOC and transferred from soil escapes to the atmosphere (3.6TgC yr^{-1}) through gas exchange kinetics (Part 1, Section 2.10). This flux is termed 'CO_2 evasion' in Fig. 2 of this study. Carbon that survives the inland water reactor is exported to the coastal ocean in the form of DOC (3.16 TgC yr^{-1}) and CO_2 (0.26 TgC yr^{-1}). These fluxes and their interpretation within the context of the Land-Ocean-Aquatic Continuum (LOAC) are returned to in Section 4.8 of this study.

4.2.1 Model Evaluation: River Discharge

Simulated river water discharge captures the key feature of Arctic river discharge – that of a massive increase in flow to ~80,000 m^3s^{-1} in April-June caused by melting snow and ice, otherwise known as ice-out or spring freshet, but underestimates observed river discharge in late summer by around 70% (Figs. 3c, 4b). Given that DOC fluxes are almost directly proportional to river discharge in the Lena basin (Fig. 3d), this sub-optimal performance with regard to hydrology during August to October seeming to be the main cause of a substantial underestimation in simulated bulk DOC outflow. Another cause may simply be the lack of peat representation in the model, for which DOC flux concentrations in outflowing fluvial water can be very high (e.g. Frey et al., 2005; 2009: see Section 4.5.1).

In addition, the mean spring (June) discharge peak flows are slightly underestimated or out of phase in simulations (Figs. 3c, 4b) compared to observations (Ye et al., 2009): this is caused by a large amount of water throughput being simulated in May (~10,000 $m^3 s^{-1}$) in excess of observed rates. Finally, during the winter low-flow period, it seems that the model consistently under-estimates water flow-through volumes reaching the river main stem (see Fig. 3c, winter months). Although this underestimate is not severe relative to annual bulk flows, the divergence is large as a percentage of observations (see right-hand axis, Fig. 3c), and may point to an issue in how ice is represented in the model, such as the fact that solid ice inclusions in the soil column are not represented, or the possibility that much slower groundwater dynamics than those represented in the model are feeding discharge. In addition to this, the presence of a dam on the Vilui tributary of the Lena has been shown to reduce main stem winter low-flow rates by up to 90% (Ye et al., 2003), similar to the discrepancy of our low-flow rates: given that our model only simulates 'natural' hydrological flows and thus does not include dams, we expect that this effect is also at play.

Deficiencies in modelled hydrology correspond to those found in Fig. 12 of Guimberteau et al. (2018), indicating that the modifications made in this model version, which focus on the DOC cycle, have not further degraded the hydrological performance of the model, the causes of which are described below. Low simulated discharge for the Lena basin, particularly during the late summer and autumn, is consistent with prior, Pan-Arctic simulations conducted by Guimberteau et al. (2018), who ran ORCHIDEE-MICT using both the GSWP3 and CRU-NCEP v7 datasets and evaluated them over the period 1981-2007. Despite the substantially better hydrological performance of ORCHIDEE under GSWP3 climate, they described a near-systematic underestimation of summer/autumn discharge rates for both datasets over the Yukon, Mackenzie, Lena and Kolyma basins. Furthermore, the discrepancy of model output between climatological datasets was almost as large as the discrepancy between model output and observational data in that study, which analysed this in great depth, suggesting that the source of error is both a

covariate of model process representation and parameterisation, as well as the climatological datasets themselves. Model hydrological representation and empirically derived climate input data are then subject to interaction with modelled soil (e.g. infiltration), vegetation (e.g. canopy interception) and thermodynamics (e.g. freezing and consequent partitioning of water transport) from which river discharge is computed, confounding full interpretation of sources of bias, briefly described below.

Model process deficiency in this regard was identified by Guimberteau et al. (2018) as residing in an overly restrictive representation of water impermeability through frozen topsoil, which decreases the residence time of running water by directing it to surface runoff rather than subsurface flow, and in the process increases the susceptibility of the total water volume to evapotranspiration from incoming shortwave radiation. This would bias both the timing (over-partitioning of water to high runoff periods) and volume of water (low bias) reaching the river stem and its eventual discharge into the ocean, respectively, as demonstrated by model output. Guimberteau et al. (2018) suggest that representation of sub-grid-scale infiltration mechanisms under frozen conditions, such as soil freezing-drying that would enhance infiltration, be included in future, yet-to-be implemented iterations of ORCHIDEE. Furthermore, we suggest that the lack of representation of lakes in ORCHIDEE, which serve to increase the time lag between precipitation/melt and oceanic discharge, may likewise be a powerful source of bias in the timing of discharge fluxes represented by the model.

Unsurprisingly, simulated surface runoff has been shown to be strongly affected by differences in precipitation between datasets (Biancamaria et al., 2009; Fekete et al., 2004), while biases in these and evapotranspiration datasets that are used to both drive and evaluate the hydrological models, are a powerful source of water balance biases in high-latitude basins (Wang et al., 2015). Indeed, climatological dataset estimates for the spatial distribution of high latitude winter snowfall are generally problematic, owing to the low density of meteorological stations (Burke et al., 2013), wind-related issues with in-field collection and measurement that lead to systematic underestimates of snowfall rates (Yang et al., 2005), creating biases in the climatological datasets that only show up when the integrator of their model input -in this case river discharge -is modelled. In addition, the wintertime partitioning of precipitation between rain and snow, a function of 2m air temperatures in the forcing datasets, strongly affects the volume and timing of runoff (Guimberteau et al., 2018; Haddeland et al., 2011). Indeed, 69% of the spatial variance of the spring freshet has been attributed to snow water-equivalent bias during the pre-melt season (Rawlins et al., 2007). In addition, errors in forcing of soil evaporation due to inaccuracies in incoming shortwave radiation, as well as biases in the parameterisation of canopy interception -a function of simulated LAI -can lead to upward biases in evapotranspiration rates (Guimberteau et al., 2018).

4.2.2 Model Evaluation: DOC Annual Discharge

Our CTRL simulation shows that the yearly sum of DOC output to the Arctic Ocean has increased steadily over course of the 20th Century, from ~1.4Tg DOC-C yr^{-1} in 1901 to ~4Tg DOC-C yr^{-1} in 2007 (Fig. 4a). Smoothing the DOC discharge over a 30-year running mean shows that the increasing trend (Fig. 4a) over this averaging scale is almost linear, at ~0.11TgC per decade, or a net increase of 40% using this averaging scale. Empirically based estimates of total contemporary DOC entering the Laptev Sea

from Lena river discharge vary around ~2.5-5.8 TgC-DOC (Cauwet and Sidorov, 1996; Dolman et al., 2012; Holmes et al., 2012; Lara et al., 1998; Raymond et al., 2007; Semiletov et al., 2011).

Note however that modelled aggregate DOC discharge is strongly affected by the underestimation of river water discharge. Fig. 4a shows the average simulated DOC discharge (red bar) of the last decade (1998-2007) of 3.2 TgC yr^{-1}, to be compared with estimates of 3.6 TgC yr^{-1} (black bar) from Lara et al. (1998) and 5.8 TgC yr^{-1} (orange bar) from Raymond et al. (2007) and 5.7 TgC yr^{-1} from Holmes et al. (2012). The most recent and elaborate of those estimates is that of Holmes et al. (2012) who used a rating curve approach based on 17 samples collected from 2003 to 2006 and covering the full seasonal cycle, which was then applied to 10 years of daily discharge data (1999-2008) for extrapolation. Given that their estimate is also based on Arctic-GRO-1/PARTNERS data (https://www.arcticgreatrivers.org/data), which stands as the highest temporal resolution dataset to date, their estimate is likely the most accurate of the DOC discharge estimate. Compared to their average annual estimate of 5.7 TgC yr^{-1}, our simulated DOC export is low by around 43%, whose causes are discussed below.

Firstly, there is a quasi-linear positive relationship between DOC discharge and river discharge (Fig. 3d). This relation is common to Arctic rivers, as DOC loading experiences disproportionately large increases with increases in discharge (Fig. 4, Raymond et al., 2007), owing largely to the 'flushing' out of terrestrially fixed carbon from the previous year's production by the massive runoff generated by ice and snow melt during the spring thaw. Comparing simulated annual mean discharge rate (m^3 s^{-1}) with long-term observations (Ye et al. 2003) over years 1940-2000 (Fig. 4c) shows that though absolute discharge rates are underestimated by simulations, their interannual variation reasonably tracks the direction and magnitude of observations. Linear regressions through each trend yield very similar yearly increases of 29 vs 38 m^3 s^{-1} yr^{-1} for simulations and observations, respectively. The observed vs. simulated mean annual water discharge differential hovers at 36% (Figs. 3d, 4c), close to the 43% differential between observed and simulated DOC discharge, giving some indication that, given the linear relationship between water and DOC discharge, most of the DOC discrepancy can be explained by the performance of the hydrology and not the DOC module, the latter of which was the subject of developments added in ORCHIDEE M-L. Applying the regression slope of the relationship in Fig. 3d (9E-06 mgC per m^3s^{-1}) to the mean river discharge discrepancy of 36%, we find that 84% of the differential between observed and simulated discharge can be explained by the underperformance of the hydrology module.

Further sources of error are process exclusion and representation/forcing limitations. Indeed, separate test runs carried out using a different set of climatological input forcing show that changing from the GSWP3 input dataset to input from bias-corrected projections from the IPSL Earth System Model under the second Inter-Sectoral Impact Model Intercomparison Project (ISIMIP2b (Frieler et al., 2017; Lange, 2016, 2018)) protocol increases DOC discharge to the ocean to 4.14 TgC yr^{-1} (+37%), largely due to somewhat higher precipitation rates in that forcing dataset (see Table S3). Thus, the choice of input dataset itself introduces a significant degree of uncertainty to model output.

In addition, this model does not include explicit peatland formation and related dynamics, which is the subject of further model developments (Qiu et al., 2018) yet to be included in this iteration. With peatlands thought to cover ~17% of the Arctic land surface (Tarnocai et al., 2009), and with substantially higher leaching concentrations, this may be a significant omission from our model. The remaining biases likely arise from errors in the interaction of simulated NPP, respiration and DOC production and decomposition, which will impact on the net in and out -flow of dissolved carbon to the fluvial system. However, the DOC relationship with these variables is less clear-cut than with river discharge. Indeed, regressions (Fig. 3e) of annual DOC versus NPP (TgC yr^{-1}) show that DOC is highly sensitive to increases in NPP, but is less coupled to it (more scattered, R^2=0.42) than other simulated fluvial carbon variables shown, i.e. aquatic CO_2 evasion and soil CO_2 export to the river network. The differences in correlation and slope of the variables in Fig. 3e are expected: aquatic CO_2 evasion is least sensitive yet most tightly coupled to NPP (R^2=0.52), while CO_2 export to rivers is intermediate between the two (R^2=0.43). The greater correlation with NPP of DOC compared to evasion is understandable, given that DOC leaching is a covariate of both NPP and runoff, whereas evasion flux is largely dependent on organic inputs (production) and temperature (see Part 1).

4.2.3 Model Evaluation: DOC Discharge Seasonality

Figure 4b shows that the bulk of the DOC outflow occurs during the spring freshet or snow/ice-melting period of increased discharge, accounting for ~50-70% of the total Arctic outflow (Lammers et al., 2001; Ye et al., 2009), with peak water discharge rates in June of ~80,000 m^3 s^{-1}. DOC concentrations increase, as meltwater flushes out DOC accumulated from the previous year's litter and SOC generation (Raymond et al., 2007; Kutscher et al., 2017). This is reproduced in our simulations, since DOC discharge peak occurs at the onset of the growing season, meaning it is generated from a temporally prior stock of organic carbon. Simulation of the hydrological dynamic is presented in maps of river discharge through the basin in Fig. 3b, which show low-flows in April with substantial hydrographic flow from upstream mountainous headwaters and Lake Baikal inflow in the south, peak flow in June dominated by headwaters, and little headwater input in September.

In Fig. 4b we observe the following: (i) DOC discharge fluxes closely track hydrological fluxes. (ii) The simulated modern river discharge peak approximates the historical observed discharge peak, but slightly overestimates spring fluxes and substantially underestimates fluxes in the autumn, as explained above. (iii) The difference between the first and last decades of the simulation in Fig. 4b is mostly attributable to a large increase in the DOC flux mobilised by spring freshet waters. This suggests both greater peaks in simulated DOC flux and a shift to earlier peak timing, owing to an increase in river discharge, indicative of an earlier spring and a progressively warmer environment over the 20th Century. (iv) The maximum modelled modern monthly DOC flux rate of ~1.3 TgC $month^{-1}$ is comparable to the mean maximum DOC flux rate measured in a recent study (1.75 TgC $month^{-1}$, Kutscher et al., 2017, Fig. 2).

We compare the Raymond et al. (2007) modern DOC outflow (Fig. 4d, solid black line) from the Lena river at Zhigansk (Raymond et al., 2007) against simulated DOC outflow from both Zhigansk and Kusur (Fig. 4d). Simulated DOC flux is underestimated for both

sites. Peakflow at Zhigansk seems to be attenuated over May and June in simulations, as opposed to May peakflow in observations. Peakflow at Kusur is definitively in June. This suggests that simulated outflow timing at Zhigansk may slightly delayed, causing a split in peak discharge when averaged in the model output. Thus the aggregation of model output to monthly averages from calculated daily and 30 minute timesteps can result in the artificial imposition of a normative temporal boundary (i.e. month) on a continuous series. This may cause the less distinctive 'sharp' peak seen in Fig. 4d, ,which is instead simulated at the downstream Kusur site, whose distance some 500km away from Zhigansk more clearly explains the delay difference in seasonality. We further evaluate our DOC discharge at the sub-basin scale, to test whether the fractional contribution of different DOC flows from each sub-basin correspond to those in their observed correlates from Kutscher et al., (2017). This comparison is depicted in Fig. S2, where the observed and simulated percentage DOC contributions of the Aldan, Vilui, and Upper and Lower Lena sub-basins to total flux rates are 19 (24)%, 20(10%), 33 (38%) and 30 (28)% in simulations (observations) for the four sub-basins, respectively. While deviations between simulated and observed DOC fluxes can be expected, the nearly twofold value mismatch of the Vilui basin is due to its real-word damming, not represented here. On the other hand, we cannot explain the ~5% discrepancies in other sub-basin fluxes, particularly for the Aldan.

4.3 DOC Concentrations in lateral transport

While total DOC discharge captures the integral of biogeochemical processes leading tha fluvial outflow, simulations of this are highly sensitive to the performance of modelled hydrology and climatological input data. A more precise measure for the performance of the newly-introduced DOC production and transport module, which is less sensitive to reproduction of river water discharge, is DOC concentration. This is because while the total amount of DOC entering river water depends on the amount of water available as a vehicle for this flux (hydrology), the concentration of DOC depends on the rate of soil carbon leaching, itself depending largely on the interaction of soil biogeochemistry with primary production and climatic factors. This we evaluate in Figure 5a, This shows that for the majority of the thaw period or growing season (April-September), which corresponds to the period during which over 90% of DOC production and transport occurs, the model largely tracks the observed seasonality of DOC concentrations in Arctic-GRO data averaged over 1999-2007. There is a large overestimate of the DOC concentration in May owing to inaccuracies in simulating the onset of the thaw period, while the months June-September underestimate concentrations by an average of 18%. On the other hand, frozen period (November-April) DOC concentrations are underestimated by between ~30-500%. This is due to deficiencies in representing wintertime soil hydrological water flow in the model, which impedes water flow when the soil is frozen, as discussed in Section 4.2.1. Because of this deficiency, slow-moving groundwater flows that contain large amounts of DOC leachate are under-represented. This interpretation is supported by the fact that in both observations and simulations, at low discharge rates (corresponding to wintertime), DOC concentrations exhibit a strong positive correlation with river discharge, while this relationship becomes insignificant at higher levels of river discharge (Fig. 5b). Thus wintertime DOC concentrations suffer from the same deficiencies in model representation as those for water discharge. In other words, the standalone representation of DOC leaching is satisfactory, while when it is sensitive to river discharge, it suffers from the same shortfalls identified in Section

441 4.2.1 and 4.2.2.
442
443 The spatial distribution of DOC concentrations are shown in maps of mean monthly DOC
444 concentration for stream water, river water and groundwater (Fig. 6a,b,c, respectively)
445 in April, June and September. For both the stream and river water reservoirs, DOC
446 concentrations appear to have spatio-temporal gradients correlated with the flux of
447 water over the basin during the thaw period, with high concentrations of 10-15 mgC L^{-1}
448 driven by April meltwaters upstream of the basin, these high concentrations moving
449 northward to the coldest downstream regions of the basin in June. Lower DOC
450 concentrations of ~5 mgC L^{-1} dominate the basin in September when the bulk of
451 simulated lateral flux of DOC has dissipated into the Laptev Sea. In contrast,
452 groundwater DOC concentrations are generally stable with time, although some pixels
453 appear to experience some 'recharge' in their concentrations during the first two of the
454 three displayed thaw months. Significantly, highest groundwater DOC concentrations of
455 up to 20 mgC L^{-1} are focussed on the highest elevation areas of the Lena basin on its
456 Eastern boundary, which are characterized by a dominance of Podzols (SI, Fig. 2b). This
457 region, the Verkhoyansk range, is clearly visible as the high groundwater DOC
458 concentration (2-20mgC L^{-1}) arc (in red) in Fig. 6a, as well as other high elevation areas
459 in the south-western portion of the basin (Fig. 3a), while the low-lying central basin
460 shows much smaller groundwater DOC concentrations (0-2mgC L^{-1}). The range of
461 simulated groundwater DOC concentration comes close to those aggregated from the
462 empirical literature by Shvartsev (2008), which finds from >9,000 observations that
463 groundwater in permafrost regions exhibit a mean concentration of ~10 mgC L^{-1} after
464 peatlands and swamps (not simulated here) are removed (Table 2).
465
466
467 **4.4 In-Stream CO_2 Production, Transport, Evasion**
468
469 In our model, the fate of DOC once it enters the fluvial system is either to remain as DOC
470 and be exported to the ocean, or to be degraded to dissolved CO_2 ($CO_{2(aq.)}$), which is
471 itself either also transported to the marine system or outgassed from the fluvial surface
472 to the atmosphere (see Part 1, Section 2.10). The latter two outcomes also apply to
473 $CO_{2(aq.)}$ produced in the soil by organic matter degradation and subsequently
474 transported by runoff and drainage flows to the water column. As shown in Fig. 2, a
475 large proportion of DOC (38%, 2.1 TgC yr^{-1}) that enters the water column is degraded to
476 $CO_{2(aq.)}$ during transport, which adds to the 1.65 TgC yr-1 of direct $CO_{2(aq.)}$ input from the
477 terrestrial land surface. Of this bulk CO_2 exported into and generated within the water
478 column, 3.6 TgC yr^{-1} evades from the water surface to the atmosphere before reaching
479 the river delta. In what follows, we evaluate first inputs of $CO_{2(aq.)}$ to the water column in
480 terms of their seasonality, before evaluating CO_2 evasion rates and the relation of this to
481 smaller and larger water bodies (river versus stream). As noted in Part 1 of this study,
482 although the model as a whole conducts simulations at the 1 degree scale, the routing of
483 water and carbon, as well as the evasion of the latter, occurs at the sub-grid scale, such
484 that we are able to simulate spatially explicit rivers whose size approximates Strahler
485 order 4, and through the 'fast' water pool in the model are able to simulate streams of
486 Strahler order 1-3.
487
488 The seasonality of riverine dissolved CO_2 concentrations ($CO_{2(aq.)}$, mgC L^{-1}) is evaluated
489 in Fig. 4d to compare $CO_{2(aq.)}$ concentrations with DOC bulk flows, since $CO_{2(aq.)}$

concentrations follow an inverse seasonal pattern to those of DOC, being highest during the winter baseflow period and lowest in summer due to dilution during its high discharge phase (Semiletov et al., 2011). The simulated flow of $CO_{2(aq.)}$ at Kusur (Fig. 4d, dashed red) reproduces the seasonality of observations from Cauwet and Sidorov (1996), who sampled the Lower Lena (Fig. 3a), but somewhat underestimates concentrations. Also included in Fig. 4d is the basin average for all non-zero values, whose shape also tracks that of observations. Thus the model represents on the one hand increasing hydrological flow mobilising increasing quantities and concentrations of DOC while on the other hand those same increasing hydrological flows increasing the flux, but decreasing the concentration, of $CO_{2(aq.)}$ throughput.

To our knowledge, no direct measurements for CO_2 evasion from the surface of the Lena river are available in the literature. We refer to Denfeld et al. (2013) for evaluating our evasion flux results, since their basin of study, the Kolyma River, is the most geographically proximate existing dataset to the Lena, despite biogeographical differences between the two basins –namely that the Kolyma is almost entirely underlain by continuous permafrost. The Kolyma River CO_2 evasion study measured evasion at 29 different sites along the river basin (~158-163°E; 68-69.5°N), with these sites distinguished from one another as 'main stem', 'inflowing river' or 'stream' on the basis of reach length. The study showed that during the summer low-flow period (August), areal river mainstem CO_2 evasion fluxes were ~0.35 gC m^{-2} d^{-1}, whereas for streams of stream order 1-3 (widths 1-19m), evasion fluxes were up to ~7 gC m^{-2} d^{-1}, and for non-mainstem rivers (widths 20-400m) mean net fluxes were roughly zero (Table 3 of Denfeld et al., 2013). Thus, while small streams have been observed to contribute to roughly 2% of the Kolyma basin surface area, their measured percentage contribution to total basin-wide CO_2 evasion ~40%, whereas for the main stem the surface area and evasion fractions were ~80% and 60%, respectively. Likewise, mean annual evasion rates of <0.8 up to around 7 gC m^{-2} d^{-1} have been found for the Ob and Pur rivers in Western Siberia (Serikova et al., 2018).

Results such as these, in addition to permafrost soil incubation experiments (e.g. Drake et al., 2015; Vonk et al., 2013, 2015b, 2015a) suggest that small streams, which represent the initial (headwater) drainage sites of these basins, rapidly process hydrologically leached carbon to the atmosphere, and that this high-reactivity carbon is a mix of recently thawed ancient permafrost material, as well as decomposing matter from the previous growth year. This is given as evidence that the total carbon processing of high-latitude rivers is significantly underestimated if only mainstem carbon concentrations are used in the accounting framework, since a large amount of carbon is metabolised to the atmosphere before reaching the site of measurement.

Figure 7 summarises some of the results from the simulated water body CO_2 outgassing flux. Year-on-year variation in basin-wide evasion from river, stream and floodplain sources combined exhibits a marked increasing trend over the course of the 20th Century, increasing from a minimum of ~1.6 $TgCO_2$-C yr^{-1} in 1901 to a maximum of ~4.4 $TgCO_2$-C yr^{-1} in 2007 (+300%) (Fig. 7a). Smoothing the data over a 30 year running average yields a dampened net increase in basin-wide evasion of ~30% (Fig. 7a). Thus yearly evasion flux is some 105% of yearly DOC discharge to the coast from the Lena basin and 51% of C exported from soils to headwaters as CO_2 or DOC. If we compare the mean yearly rate of increase in absolute (TgC yr^{-1}) CO_2 evasion and DOC discharge based

on linear regression over the whole simulation period, it appears that the rate of increase of both fluxes has been strikingly similar over the simulated 20th Century, with mean increases of 11.1 GgC yr^{-1} and 11.5 GgC yr^{-1} per year for evasion and export, respectively.

The heterogeneity of CO_2 evasion from different sources in the model is most evident in terms of their geographic distribution and relative intensity, as shown in the evasion flux rate maps over stream and river areas in April, June and September (Fig. 8a-b). Stream evasion (Fig.8a), tends to be broadly distributed over the whole basin, representing the fact that small streams and their evasion are the main hydrologic connectors outside of the main river and tributary grid cells, whereas river evasion (Fig. 8b) is clearly linked to the hydrographic representation of the Lena main stem itself, with higher total quantities in some individual grid cells than for the stream reservoir, yet distributed amongst a substantially smaller number of grid cells. Whereas the stream reservoir has greatest absolute evasion flux rates earlier in the year (April-May), maximum evasion rates occur later in the year and further downstream for the river reservoir, reflecting the fact that headwaters are first-order integrators of soil-water carbon connectivity, whereas the river mainstem and tributaries are of a secondary order.

The spatio-temporal pattern of increasing evasion over the simulation period is shown in Fig. 7b as a Hovmöller difference plot, between the last and first decade, of log-scale average monthly evasion rates per latitudinal band. This shows that the vast majority of outgassing increase occurs between March and June, corresponding to the progressive onset of the thaw period moving northwards over this timespan. Although relatively small, outgassing increases are apparent for most of the year, particularly at lower latitudes. This would suggest that the change is driven most acutely by relatively greater temperature increases at higher latitudes ('Arctic amplification' of climate warming, e.g. Bekryaev et al., 2010) while less acute but more temporally homogenous evasion is driven by seasonal warming at lower latitudes.

As previously discussed, the proportion of total basin-wide CO_2 evasion attributable to headwater streams and rivers is substantially greater than their proportion of total basin surface area. Figure 7c represents the mean monthly fractional contribution of each surface hydrological water pool to the total evasion flux (unitless) over the period 1998-2007. This shows that over the entirety of the thaw period, the stream water pool takes over from the river water pool as the dominant evasion source, particularly at the height of the freshet period, where its fractional contribution rises to >75%.

The stream fraction of August outgassing is ~57% of the annual total, which is higher than the ~40% found for streams in the Denfeld et al. (2013) study. However, the values between the two studies are not directly comparable, different basins notwithstanding. This is because in ORCHIDEE MICT-L, the 'stream' water reservoir is water routed to the river network for all hydrologic flows calculated to not cross a 0.5 degree grid cell boundary (the resolution of the routing module, explained in Part 1, Section 2.6), which may not be commensurate with long, <20m width streams in the real-world, that were used in the Denfeld et al. (2013) study. In addition, this 'stream' water reservoir in the model does not include any values for width or area in the model, so we cannot directly compare our stream reservoir to the <20m width criterion

588 employed by Denfeld et al. (2013) in their definition of an observed stream. Thus our
589 'stream' water reservoir encompasses substantially greater surface area and hydrologic
590 throughput than that in the Denfeld et al. study. Also shown in Fig. 7c is the gradual
591 onset of evasion from the floodplain reservoir in April, as the meltwater driven surge in
592 river outflow leads to soil inundation and the gradual increase of proportional evasion
593 from these flooded areas over the course of the summer, with peaks in June-August as
594 water temperatures over these flooded areas likewise peak. We stress the importance
595 of these simulation results as they concur with large numbers of observational studies
596 (cited above) which show smaller headwater streams' disproportionately large
597 contribution to total outgassing (Fig. 7c), this being due to their comparatively high
598 outgassing rates (Fig. 7e). In addition, the contribution of floodplains to evasion, an
599 otherwise rarely studied feature of high latitude biomes, is shown here to be significant.
600
601 A Hovmöller plot (Fig. 7d) of the monthly longitude-averaged stream reservoir fraction
602 of total evasion, allows us to infer that: (i) The dominance of stream evasion begins in
603 the most southern upstream headwaters in the lower latitude thaw period (April-May),
604 and trickles northward over the course of the next two months, following the riverflow.
605 (ii) The intensity of this evasion is greatest in the lower latitude regions of the basin,
606 which we speculate is the result of higher temperatures causing a greater proliferation
607 of small thaw water-driven flows and evasion. (iii) Areas where the stream fraction is
608 not dominant or only briefly dominant during the summer (58-60°N, 63-64°N, 70-71°N)
609 are all areas where floodplain CO_2 evasion plays a prominent role at that latitudinal
610 band.
611
612 We evaluate the approximate rate of modelled areal CO_2 efflux from the water surface
613 against observations from Denfeld et al. (2013). The 'approximate' caveat refers to the
614 fact that model output doesn't define a precise surface area for the stream water
615 reservoir, which is instead bundled into a single value representing the riverine fraction
616 of a grid cell's total surface area. To approximate the areal outgassing for the stream
617 versus river water reservoirs, we weight the total non-floodplain inundated area of each
618 grid cell by the relative total water mass of each of the two hydrological pools, then
619 divide the total daily CO_2 flux simulated by the model by this value. The per-pool areal
620 estimate is an approximation since it assumes that rivers and streams have the same
621 surface area: volume relationship. This is clearly not the case, since streams are
622 generally shallow, tending to have greater surface area per increment increase in depth
623 than rivers. Thus, our areal approximations are likely underestimated (overestimated)
624 for streams (rivers), respectively.
625
626 The comparison of simulated results with those from Denfeld et al. (2013) are displayed
627 in Fig. 7e, which shows boxplots for simulated CO_2 evasion from the stream water
628 reservoir and river water reservoir averaged over 1998-2007. The empirical (Kolyma
629 river) analogue of this data, from which this plot is inspired (Fig. 4d in Denfeld et al.,
630 2013), is shown inset in the figure, with whiskers in their case denoting measured
631 maxima and minima. Median efflux was 1.1 (6) versus 0.4 (0.8) for stream and river,
632 respectively, in simulations (observations). Like the observations, simulated stream
633 efflux had a substantially greater interquartile range, mean (24.6) and standard
634 deviation (73) than total river efflux (1.3 and 7.2, respectively). Note that from ~700
635 non-zero simulation datapoints, 7 were omitted as 'outliers' from the stream reservoir
636 efflux statistics described below, because very low stream:river reservoir values skewed

the estimation of total approximate stream surface area values very low, leading to extreme efflux rate values of 1-3000gC m^{-2} d^{-1} and are thus considered numerical artefacts of the areal approximation approach used here.

4.5 Emergent Phenomena

4.5.1 DOC and mean annual air temperature

A key emergent property of DOC concentrations in soils and inland waters should be their positive partial determination by the temperature of the environment under which their rates of production occur, as has been shown in the literature on permafrost regions, most notably in Frey & Smith (2005) and Frey & McClelland (2009).

Increasing temperatures should lead to greater primary production, thaw, decomposition and microbial mobilisation rates, and hence DOC production rates, leading to (dilution effects notwithstanding) higher concentrations of DOC in thaw and so stream waters. Looking at this emergent property allows us to evaluate the soil-level production of both DOC and thaw water at the appropriate biogeographic and temporal scale in our model. This provides a further constraint on model effectiveness at simulating existing phenomena at greater process-resolution.

Figure 9 compares three datasets (simulated and two observational) of riverine DOC concentration (in mgC L^{-1}) plotted against mean annual air temperature (MAAT). The simulated grid-scale DOC versus MAAT averaged over July and August (for comparability of DOC with observational sampling period) of 1998-2007 is shown in red, and observed data compiled by Laudon et al. (2012) and Frey and Smith (2005) for sites in temperate/cold regions globally and peatland-dominated Western Siberia, respectively. The Laudon et al. (2012) data are taken from 49 observations including MAAT over the period 1997-2011 from catchments north of 43°N, and aggregated to 10 regional biogeographies, along with datapoints from their own sampling; those in the Frey and Smith study are from 55-68°N and ~65-85°E (for site locations, see Laudon et al. (2012), Table 1 and 2; Frey and Smith (2005), Fig. 1).

Fig. 9 can be interpreted in a number of ways. First, this MAAT continuum spans the range of areas that are both highly and moderately permafrost affected and permafrost free (Fig. 9, blue and green versus orange shading, respectively), potentially allowing us a glimpse of the behaviour of DOC concentration as the environment transitions from the former to the latter. Simulated Lena DOC concentrations, all in pixels with MAAT < -2°C and hence all bearing continuous or discontinuous permafrost ('permafrost-affected' in the figure), only exhibit a weakly positive response to MAAT on the scale used ($y=6.05e^{0.03MAAT}$), although the consistent increase in DOC minima with MAAT is clearly visible. Second, the Laudon et al. (2012) data exhibit an increasing then decreasing trend over the range of MAAT (-2°C to 10°C) in their dataset, which they propose reflects an 'optimal' MAAT range (0-3°C) for the production and transport of DOC (Fig. 9, red shading). Below this optimum range, DOC concentrations may be limited by transport due to freezing, and above this, smaller soil carbon pools and temperature-driven decomposition would suppress the amount of DOC within rivers. Third, the lower end of the Laudon et al. (2012) MAAT values correspond to a DOC concentration in line with DOC concentrations simulated by our model. Fourth, DOC concentrations in the Frey and Smith (2005) data exhibit a broad scattering in

permafrost-affected sites, with concentrations overlapping those of our simulations (Fig. 9, green shading), before rapidly increasing to very high concentrations relative to the Laudon et al. (2012) data, as sites transition to permafrost-free (red shading, $y=3.6_{MAAT}+29.4$).

Their data highlight the difference in DOC concentration regime between areas of high (Frey and Smith, 2005) and low (Laudon et al., 2012) peatland coverage and the different response of these to temperature changes. Fifth, because our simulation results largely correspond with the observed data where the MAAT ranges overlap (green shading), and because our model lacks peatland processes, we should expect our model to follow the polynomial regression plotted for the Laudon et al. (2012) data as temperature inputs to the model increase. Figure 9 implies that this increase should be on the order of a doubling of DOC concentration as a system evolves from a MAAT of -2°C to 2°C. With warming, we expect the response of DOC concentrations to reflect a mix of both observationally-derived curves, as a function of peatland coverage.

4.5.2 DOC and topographic slope

Subsurface water infiltration fluxes and transformations of dissolved matter represent an important, if poorly understood and observationally under-represented biogeochemical pathway of DOC export to river main stems, involving the complex interplay of slope, parent material, temperature, permafrost material age and soil physical-chemical processes, such as adsorption and priming. In the Lena basin, as in other permafrost catchments, topographic slope has been shown to be a powerful predictor for water infiltration depth, and concentration and age of DOC (Jasechko et al., 2016; Kutscher et al., 2017; McGuire et al., 2005), with deeper flow paths and older, lower DOC-concentrated waters found as the topographic slope increases. This relationship was shown in Fig. 4 of Kutscher et al. (2017) who surveyed DOC concentrations across a broad range of slope angle values in the Lena basin and found a distinct negative relationship between the two. Comparing the Kutscher et al. (2017) values with our model output, by plotting stream and river DOC concentrations averaged per gridpoint over 1998-2007 against the topographic map used in the routing scheme (Fig. 10) we find a similar negative relationship between the two variables.

This relationship was found in temperate rivers by Lauerwald et al. (2012), and in a recent Pan-Arctic synthesis paper Connolly et al. (2018). The reasoning for the negative slope-DOC concentration relationship is that as elevation increases, temperature and primary production decreases. This leads to a thinner organic soil layer, meaning that mineral soil plays a stronger role in shallow hydrologic flowpaths, allowing for deeper infiltration and shorter residence time in a given soil layer. Further, steeper terrain leads to a lower soil water residence time and lower moisture than in flat areas. As a result, a given patch of soil matter will be exposed to leaching for less (residence) time, while the organic matter that is leached is thought to be adsorbed more readily to mineral soil particles, leading to either their re-stabilisation in the soil column or shallow retention and subsequent heterotrophic respiration in situ, cumulatively resulting in lower DOC concentrations in the hydrologic export (Kaiser and Kalbitz, 2012; Klaminder et al., 2011). This line of reasoning was recently shown to apply also to deep organic permafrost soils (Zhang et al., 2017), although the degree to which this is the case in comparison to mineral soils is as yet unknown.

In addition, and as described in Part 1 (Section 2.5) of this study, MICT-L contains a provision for increased soil column infiltration and lower decomposition rates in areas underlain by Podzols and Arenosols. The map from the Harmonized World Soil Database (Nachtergaele, 2010), which is used as the input to this criterion, shows areas underlain by these soils in the Lena basin to also be co-incident with areas of high topographic slope (Fig. 3a, SI, Fig S3b). The 'Podzol effect' is to increase the rate of decomposition and infiltration of DOC, relative to all other soil types, thus also increasing the rate of DOC flux into groundwater (see Part 1 of this study, Section 2.5). Thus, our modelling framework explicitly resolves the processes involved in these documented dynamics – soil thermodynamics, solid vertical flow (turbation), infiltration as a function of soil textures and types, adsorption as a function of soil parameters (see Part 1 of this study, Section 2.11), DOC respiration as a function of soil temperature and hence depth (Part 1, Section 2.12), and lagging of DOC vertical flow behind hydrological drainage flow (summary Figure in Part 1, Fig. 1). We thus have some confidence in reporting that the simulated negative relationship of DOC concentration with topographic slope may indeed emerge from the model.

4.6 DOC Reactivity Pools

Here we examine the reactivity of DOC leached from the soil and litter to different hydrological export pools. Surface runoff DOC export is dominated by refractory carbon (Fig. 11a), with export rates largely following discharge rates as they drain the basin with an increasing delay when latitude increases. As the thaw period gets underway (April), the fraction of labile carbon in surface runoff DOC increases substantially from south to north, reflecting the hydrologic uptake of the previous year's un-decomposed high-reactivity organic matter.

Refractory C–dominated drainage DOC export (Fig. 11a) is highest in June through October, with refractory export rate intensities per latitudinal band during this period consistent with the fraction of inundated area (Fig. S1b) over these bands during the year. The high refractory proportion of drainage flow is expected, as drainage leaches older, relict soil and litter matter. Because of its longer residence time within the soil column, labile DOC carried downward via soil infiltration will tend to be metabolised in situ before it can be exported to the hydrological network, further increasing the proportion of refractory carbon. By contrast floodplain DOC export (Fig. 11a) is composed of more nuanced mix of both reactivity classes, reflecting its relatively greater dependence on the current year's 'fresh' biomass as source material (62% labile DOC versus 38% refractory DOC, year-averaged) for carbon leaching.

For both the river and stream pool, mean DOC concentrations are dominated by refractory carbon sources. When averaged over the year, the dominance of the refractory DOC carbon pool over its labile counterpart is also evident for all DOC inputs to the hydrological routing except for floodplain inputs, as well as within the 'flowing' stream and river pools themselves. This is shown in Table 2, where the year-averaged percentage of each carbon component of the total input or reservoir is subdivided between the 'North' and 'South' of the basin, these splits being arbitrarily imposed as the latitudinal mid-point of the basin itself (63N). This reinforces the generalised finding from our simulations that refractory carbon dominates runoff and drainage inflows to rivers (89% refractory, on average), while floodplains export mostly labile DOC to the

784 basin (64%), these values being effectively independent of this latitudinal sub-division
785 (Table 2). Nonetheless, there is a small consistent difference between North and South
786 in stream and river water DOC makeup, in that the labile portion decreases between
787 North and South ; this may be an attenuated reflection of the portion of labile DOC that is
788 decomposed to CO_2 within the water column during its transport northward, affecting
789 the bulk average proportions contained within the water in each 'hemisphere'.
790
791 **5 Discussion**
792
793 **5.1 Land-Ocean Aquatic Continuum (LOAC)**
794 **5.1.1 LOAC Fluxes**
795
796 Overall, our simulation results show that dissolved carbon entering the Lena river
797 system is significantly transformed during its transport to the ocean. Taking the average
798 throughput of carbon into the system over the last ten years of our simulation, our
799 results show that whereas 7 TgC yr^{-1} (after reinfiltration following flooding of 0.45 TgC
800 yr^{-1}; see Fig. 2 'Return' flux) of carbon enters the Lena from terrestrial sources as
801 dissolved carbon and CO_2, only 3.4 TgC yr^{-1} is discharged into the Laptev Sea and beyond
802 from the river mouth. The remainder (3.6TgC yr^{-1}) is metabolised in the water column
803 during transport and evaded to the atmosphere (bottom panel, Fig. 12a). The terrestrial
804 DOC inflow estimate is comparable to that made by Kicklighter et al. (2013), who
805 estimated in a modelling study terrestrial dissolved carbon loading of the Lena is ~7.7
806 TgC yr^{-1}.
807
808 The relative quantities of carbon inflow, evasion and outflow in the river system that are
809 presented for the Lena in Fig. 12a can be compared to the same relative quantities –that
810 is, the ratios of evasion:in and out:in, where 'in' refers to dissolved terrestrial input, –
811 from the global study by Cole et al. (2007), who estimated these fluxes from empirical or
812 empirically-derived data at the global scale. This is shown in the top panel of Fig. 12a,
813 where we simplify the Cole et al. (2007) data to exclude global groundwater CO_2 flux
814 from the coast to the ocean (because our basin mask has a single coastal pixel whereas
815 coastal groundwater seepage is distributed along the entire continental boundary) and
816 the POC fraction of in-river transport and sedimentation (since ORCHIDEE MICT lacks a
817 POC erosion/sedimentation module) from their budget.
818
819 This gives global terrestrial dissolved carbon input of 1.45 PgC yr^{-1}, 0.7 PgC of which is
820 discharged to the ocean, and the other 0.75 PgC evaded to the atmosphere. Taking the
821 previously mentioned [evasion:in] and [out:in] ratios as a percentage, the outflow and
822 evasion fluxes for the Lena versus the global aggregate are remarkably similar, at 48.6
823 vs. 48.3% and 51.4 vs 51.7%, for the two respective flows. Thus our results agree with
824 the proposition that the riverine portion of the 'land-ocean aquatic continuum' (Regnier
825 et al., 2013) or 'boundless carbon cycle' (Battin et al., 2009) is indeed a substantial
826 reactor for matter transported along it.
827
828 **5.1.2 LOAC drivers**
829
830 The constant climate (CLIM) and constant CO_2 (CO2) simulations described in Section 3
831 were undertaken to assess the extent –and the extent of the difference –to which these
832 two factors are drivers of model processes and fluxes. These differences are

summarised in Figs. 12(b-c), in which we show the same 1998-2007 –averaged yearly variable fluxes as in the CTRL simulation, expressed as percentages of the CTRL values given in Fig. 2. A number of conclusions can be drawn from these diagrams.

First, all fluxes are lower in the factorial simulations, which can be expected due to lower carbon input to vegetation from the atmosphere (constant CO_2) and colder temperatures (constant climate) inhibiting more vigorous growth and carbon cycling. Second, broadly speaking, both climate and CO_2 appear to have similar effects on all fluxes, at least within the range of climatic and CO_2 values to which they have subjected the model in these historical runs. With regard to lateral export fluxes in isolation, variable climate (temperature increase) is a more powerful driver than CO_2 increase (see below). Third, the greatest difference between the constant climate and CO_2 simulation carbon fluxes appear to be those associated with terrestrial inflow of dissolved matter to the aquatic network, these being more sensitive to climatic than CO_2 variability. This is evidenced by a 49% and 32% decline in CO_2 and DOC export, respectively, from the land to rivers in the constant climate simulation, versus a 27% and 23% decline in these same variables in the constant CO_2 simulation. Given that the decline in primary production and respiration in both factorial simulations was roughly the same, this difference in terrestrial dissolved input is attributable to the effect of climate (increased temperatures) on the hydrological cycle, driving changes in lateral export fluxes.

This would imply that at these carbon dioxide and climatic ranges, the modelled DOC inputs are slightly more sensitive to changes in the climate rather than to changes in atmospheric carbon dioxide concentration and the first order biospheric response to this. However, while the model biospheric response to carbon dioxide concentration may be linear, thresholds in environmental variables such as MAAT may prove to be tipping points in the system's emergent response to change, as implied by Fig. 9, meaning that the Lena, as with the Arctic in general, may soon become much more temperature-dominated with regard to the drivers of its own change.

5.1.3 LOAC export flux considerations

Despite our simulations' agreement with observations regarding the proportional fate of terrestrial DOC inputs as evasion and marine export (Fig. 12a), our results suggest substantial and meaningful differences in the magnitude of those fluxes relative to NPP in the Lena, compared to those estimated by other studies in temperate or tropical biomes. Our simulations' cumulative DOC and CO_2 export from the terrestrial realm into inland waters is equivalent to ~1.5 % of NPP.

This is considerably lower than Cole et al. (2007) and Regnier et al. (2013) who find lateral transfer to approximate ~5% (1.9PgC yr^{-1}) of NPP at the global scale, while Lauerwald et al. (2017) found similar rates for the Amazon. The cause of this discrepancy with our results is beyond the scope of this study to definitively address, given the lack of tracers for carbon source and age in our model. Nonetheless, our analysis leads us to hypothesise the following.

Temperature limitation of soil microbial respiration at the end of the growing season (approaching zero by October, SI Fig. S5d) makes this flux neglible from November

through May (SI Fig. S5d). In late spring, mobilisation of organic carbon is performed by both microbial respiration and leaching of DOC via runoff and drainage water fluxes. However, because the latter are controlled by the initial spring meltwater flux period, which occurs before the growing season has had time to produce litter or new soil carbon (May-June, Fig. 4b), aggregate yearly DOC transport reactivity is characterised by the available plant matter from the previous year, which is overwhelmingly derived from recalcitrant soil matter (Fig. 11a) and is itself less available for leaching based on soil carbon residence times.

This causes relatively low leaching rates and riverine DOC concentrations (e.g. Fig. 9), as compared to the case of leaching from the same year's biological production. Highlighting this point is floodplain domination by labile carbon sourced from that year's production with a mean DOC concentration of 12.4 mgC L^{-1} (1998-2007 average), with mean riverine DOC concentrations around half that value (6.9 mgC L^{-1}). Nonetheless the May-June meltwater pulse period dominates aggregate DOC discharge. As this pulse rapidly subsides by late July, so does the leaching and transport of organic matter. Warmer temperatures come in conjunction with increased primary production and the temperature driven soil heterotrophic degradation of contemporary and older matter (via active layer deepening). These all indicate that transported dissolved matter in rivers, at least at peak outflow, is dominated by sources originating in the previous year's primary production, that was literally 'frozen out' of more complete decomposition by soil heterotrophs.

Further, we infer from the fact that all of our simulation grid cells fall within areas of low (<-2°C) MAAT, far below the threshold MAAT (>3°C) proposed by Laudon et al. (2012) for soil respiration-dominated carbon cycling systems (Fig. 9), that the Lena is hydrologically-limited with respect to DOC concentration and its lateral flux. Indeed, the seasonal discharge trend of the Lena –massive snowmelt-driven hydrological and absolute DOC flux, coupled with relatively low DOC concentrations at the river mouth (Fig. 4b, simulation data of Fig. 9), are in line with the Laudon et al. (2012) typology.

We therefore suggest that relatively low lateral transport relative to primary production rates (e.g. as a percentage of net primary production, (%NPP)) in our simulations compared to the lateral transport : NPP percentages reported from the literature in other biomes is driven by meltwater (vs. precipitation) dominated DOC mobilisation, which occurs during a largely pre-litter deposition period of the growing season. DOC is then less readily mobilised by being sourced from recalcitrant matter, leading to low leaching concentrations relative to those from labile material. As discharge rates decline, the growing season reaches its peak, leaving carbon mobilisation of fresh organic matter to be overwhelmingly driven by in situ heterotrophic respiration.

While we have shown that bulk DOC fluxes scale linearly to bulk discharge flows (Fig. 3d), DOC concentrations (mgC L^{-1}) hold a more complex and weaker positive relationship with discharge rates, with correlation coefficients (R^2) of 0.05 and 0.25 for river and stream DOC concentrations, respectively (Fig. 13). This implies that while increasing discharge reflects increasing runoff and an increasing vector for DOC leaching, particularly in smaller tributary streams, by the time this higher input of carbon reaches the river main stem there is a confounding effect of dilution by increased water fluxes which reduces DOC concentrations, explaining the difference between

stream and river discharge vs. DOC concentration regressions in the Figure. Thus, and as a broad generalisation, with increasing discharge rates we can also expect somewhat higher concentrations of terrestrial DOC input to streams and rivers. Over the floodplains, DOC concentrations hold no linear relationship with discharge rates (R^2=0.003 , SI Fig. S6), largely reflecting the fact that DOC leaching is here limited by terrestrial primary production rates more than by hydrology. To the extent that floodplains fundamentally require flooding and hence do depend on floodwater inputs at a primary level, we hypothesise that DOC leaching rates are not limited by that water input, at least over the simulated Lena basin.

As discussed above simulated DOC and CO_2 export as a percentage of simulated NPP over the Lena basin was 1.5% over 1998-2007. However, this proportion appears to be highly dynamic at the decadal timescale. As shown in Fig. S7, all lateral flux components in our simulations increased their relative throughput at a rate double to triple that of NPP or respiration fluxes over the 20th century, also doing so at a rate substantially higher than the rate increase in discharge. In addition, differentials of these lateral flux rates with the rates of their drivers (discharge, primary production) have on average increased over the century (Fig. S7). This suggests that there are potential additive effects of the production and discharge drivers of lateral fluxes that could lead to non-linear reponses to changes in these drivers as the Arctic environment transforms, as suggested by the Laudon et al. (2012) data plotted in Fig. 4. Acceleration of the hydrological cycle compounded by temperature and CO_2 -driven increases in primary production could therefore increase the amount of matter available for leaching, increase the carbon concentration of leachate, and increase the aggregate generation of runoff to be used as a DOC transport vector. Given that these causal dynamics apply generally to permafrost regions, both low lateral flux as %NPP and the hypothesised response of those fluxes to future warming may be a feature particular to most high latitude river basins.

6. Conclusion

This study has shown that the new DOC-representing high latitude model version of ORCHIDEE, ORCHIDEE MICT-LEAK, is able to reproduce with reasonable accuracy modern concentrations, rates and absolute fluxes of carbon in dissolved form, as well as the relative seasonality of these quantities through the year. When combined with a reasonable reproduction of real-world stream, river and floodplain dynamics, we demonstrate that this model is a potentially powerful new tool for diagnosing and reproducing past, present and potentially future states of the Arctic carbon cycle. Our simulations show that of the 34 TgC yr^{-1} remaining after GPP is respired autotrophically and heterotrophically in the Lena basin, over one-fifth of this captured carbon is removed into the aquatic system. Of this, over half is released to the atmosphere from the river surface during its period of transport to the ocean, in agreement with previous empirically-derived global-scale studies. Both this transport and its transformation are therefore non-trivial components of the carbon system at these latitudes that we have shown are sensitive to changes in temperature, precipitation and atmospheric CO_2 concentration. Our results, in combination with empirical data, further suggest that changes to these drivers –in particular climate –may provoke non-linear responses in the transport and transformation of carbon across the terrestrial-aquatic system's

interface as change progresses in an Arctic environment increasingly characterised by amplified warming.

Code and data availability

The source code for ORCHIDEE MICT-LEAK revision 5459 is available via http://forge.ipsl.jussieu.fr/orchidee/wiki/GroupActivities/CodeAvalaibilityPublication/ORCHIDEE_gmd-2018-MICT-LEAK_r5459

Primary data and scripts used in the analysis and other supplementary information that may be useful in reproducing the author's work can be obtained by contacting the corresponding author.

Authors' contribution

SB coded this model version, conducted the simulations and wrote the main body of the paper. RL gave consistent input to the coding process and made numerous code improvements and bug fixes. BG advised on the inclusion of priming processes in the model and advised on the study design and model configuration; DZ gave input on the modelled soil carbon processes and model configuration. PR contributed to the interpretation of results and made substantial contributions to the manuscript text. MG, AT and AD contributed to improvements in hydrological representation and floodplain forcing data. PC oversaw all developments leading to the publication of this study. All authors contributed to suggestions regarding the final content of the study.

Competing interests

The authors declare no competing financial interests.

Acknowledgements

Simon Bowring acknowledges funding from the European Union's Horizon 2020 research and innovation program under the Marie Sklodowska-Curie grant agreement No. 643052, 'C-CASCADES' program. Simon Bowring received a PhD grant. Matthieu Guimberteau acknowledges funding from the European Research Council Synergy grant ERC-2013-SyG-610028 IMBALANCE-P. RL acknowledges funding from the European Union's Horizon 2020 research and innovation program under grant agreement no.703813 for the Marie Sklodowska-Curie European Individual Fellowship "C-Leak".

References:

Battin, T. J., Luyssaert, S., Kaplan, L. A., Aufdenkampe, A. K., Richter, A. and Tranvik, L. J.: The boundless carbon cycle, Nat. Geosci., doi:10.1038/ngeo618, 2009.

Bekryaev, R. V., Polyakov, I. V. and Alexeev, V. A.: Role of polar amplification in long-term surface air temperature variations and modern arctic warming, J. Clim., doi:10.1175/2010JCLI3297.1, 2010.

Biancamaria, S., Bates, P. D., Boone, A. and Mognard, N. M.: Large-scale coupled hydrologic and hydraulic modelling of the Ob river in Siberia, J. Hydrol., doi:10.1016/j.jhydrol.2009.09.054, 2009.
Burke, E. J., Dankers, R., Jones, C. D. and Wiltshire, A. J.: A retrospective analysis of pan Arctic permafrost using the JULES land surface model, Clim. Dyn., doi:10.1007/s00382-012-1648-x, 2013.
Cauwet, G. and Sidorov, I.: The biogeochemistry of Lena River: Organic carbon and nutrients distribution, in Marine Chemistry., 1996.
Cole, J. J., Prairie, Y. T., Caraco, N. F., McDowell, W. H., Tranvik, L. J., Striegl, R. G., Duarte, C. M., Kortelainen, P., Downing, J. A., Middelburg, J. J. and Melack, J.: Plumbing the global carbon cycle: Integrating inland waters into the terrestrial carbon budget, Ecosystems, doi:10.1007/s10021-006-9013-8, 2007.
Connolly, C. T., Khosh, M. S., Burkart, G. A., Douglas, T. A., Holmes, R. M., Jacobson, A. D., Tank, S. E. and McClelland, J. W.: Watershed slope as a predictor of fluvial dissolved organic matter and nitrate concentrations across geographical space and catchment size in the Arctic, Environ. Res. Lett., 13(10), 104015, doi:10.1088/1748-9326/aae35d, 2018.
DeLuca, T. H. and Boisvenue, C.: Boreal forest soil carbon: Distribution, function and modelling, Forestry, doi:10.1093/forestry/cps003, 2012.
Denfeld, B., Frey, K. and Sobczak, W.: Summer CO 2 evasion from streams and rivers in the Kolyma River basin, north-east Siberia, Polar …, doi:10.3402/polar.v32i0.19704, 2013.
Dolman, A. J., Shvidenko, A., Schepaschenko, D., Ciais, P., Tchebakova, N., Chen, T., Van Der Molen, M. K., Belelli Marchesini, L., Maximov, T. C., Maksyutov, S. and Schulze, E. D.: An estimate of the terrestrial carbon budget of Russia using inventory-based, eddy covariance and inversion methods, Biogeosciences, doi:10.5194/bg-9-5323-2012, 2012.
Drake, T. W., Wickland, K. P., Spencer, R. G. M., McKnight, D. M. and Striegl, R. G.: Ancient low–molecular-weight organic acids in permafrost fuel rapid carbon dioxide production upon thaw, Proc. Natl. Acad. Sci., doi:10.1073/pnas.1511705112, 2015.
Fekete, B. M., Vörösmarty, C. J., Roads, J. O. and Willmott, C. J.: Uncertainties in precipitation and their impacts on runoff estimates, J. Clim., doi:10.1175/1520-0442(2004)017<0294:UIPATI>2.0.CO;2, 2004.
Frey, K. E. and McClelland, J. W.: Impacts of permafrost degradation on arctic river biogeochemistry, Hydrol. Process., doi:10.1002/hyp.7196, 2009.
Frey, K. E. and Smith, L. C.: Amplified carbon release from vast West Siberian peatlands by 2100, Geophys. Res. Lett., doi:10.1029/2004GL022025, 2005.
Frieler, K., Lange, S., Piontek, F., Reyer, C. P. O., Schewe, J., Warszawski, L., Zhao, F., Chini, L., Denvil, S., Emanuel, K., Geiger, T., Halladay, K., Hurtt, G., Mengel, M., Murakami, D., Ostberg, S., Popp, A., Riva, R., Stevanovic, M., SuzGBRi, T., Volkholz, J., Burke, E., Ciais, P., Ebi, K., Eddy, T. D., Elliott, J., Galbraith, E., Gosling, S. N., Hattermann, F., Hickler, T., Hinkel, J., Hof, C., Huber, V., Jägermeyr, J., Krysanova, V., Marcé, R., Müller Schmied, H., Mouratiadou, I., Pierson, D., Tittensor, D. P., Vautard, R., Van Vliet, M., Biber, M. F., Betts, R. A., Leon Bodirsky, B., Deryng, D., Frolking, S., Jones, C. D., Lotze, H. K., Lotze-Campen, H., Sahajpal, R., Thonicke, K., Tian, H. and Yamagata, Y.: Assessing the impacts of 1.5â€°C global warming - Simulation protocol of the Inter-Sectoral Impact Model Intercomparison Project (ISIMIP2b), Geosci. Model Dev., doi:10.5194/gmd-10-4321-2017, 2017.
Guimberteau, M., Zhu, D., Maignan, F., Huang, Y., Yue, C., Dantec-N d lec, S., Ottl, C., Jornet-Puig, A., Bastos, A., Laurent, P., Goll, D., Bowring, S., Chang, J., Guenet, B., Tifafi, M., Peng, S., Krinner, G., Ducharne, A. s., Wang, F., Wang, T., Wang, X., Wang, Y., Yin, Z., Lauerwald,

R., Joetzjer, E., Qiu, C., Kim, H. and Ciais, P.: ORCHIDEE-MICT (v8.4.1), a land surface model for the high latitudes: model description and validation, Geosci. Model Dev., doi:10.5194/gmd-11-121-2018, 2018.
Haddeland, I., Clark, D. B., Franssen, W., Ludwig, F., Voß, F., Arnell, N. W., Bertrand, N., Best, M., Folwell, S., Gerten, D., Gomes, S., Gosling, S. N., Hagemann, S., Hanasaki, N., Harding, R., Heinke, J., Kabat, P., Koirala, S., Oki, T., Polcher, J., Stacke, T., Viterbo, P., Weedon, G. P. and Yeh, P.: Multimodel Estimate of the Global Terrestrial Water Balance: Setup and First Results, J. Hydrometeorol., doi:10.1175/2011JHM1324.1, 2011.
Holmes, R. M., McClelland, J. W., Peterson, B. J., Tank, S. E., Bulygina, E., Eglinton, T. I., Gordeev, V. V., Gurtovaya, T. Y., Raymond, P. A., Repeta, D. J., Staples, R., Striegl, R. G., Zhulidov, A. V. and Zimov, S. A.: Seasonal and Annual Fluxes of Nutrients and Organic Matter from Large Rivers to the Arctic Ocean and Surrounding Seas, Estuaries and Coasts, doi:10.1007/s12237-011-9386-6, 2012.
Jasechko, S., Kirchner, J. W., Welker, J. M. and McDonnell, J. J.: Substantial proportion of global streamflow less than three months old, Nat. Geosci., doi:10.1038/ngeo2636, 2016.
Kaiser, K. and Kalbitz, K.: Cycling downwards - dissolved organic matter in soils, Soil Biol. Biochem., doi:10.1016/j.soilbio.2012.04.002, 2012.
Kalnay, E., Kanamitsu, M., Kistler, R., Collins, W., Deaven, D., Gandin, L., Iredell, M., Saha, S., White, G., Woollen, J., Zhu, Y., Chelliah, M., Ebisuzaki, W., Higgins, W., Janowiak, J., Mo, K. C., Ropelewski, C., Wang, J., Leetmaa, A., Reynolds, R., Jenne, R. and Joseph, D.: The NCEP/NCAR 40-year reanalysis project, Bull. Am. Meteorol. Soc., doi:10.1175/1520-0477(1996)077<0437:TNYRP>2.0.CO;2, 1996.
Kicklighter, D. W., Hayes, D. J., Mcclelland, J. W., Peterson, B. J., Mcguire, A. D. and Melillo, J. M.: Insights and issues with simulating terrestrial DOC loading of Arctic river networks, Ecol. Appl., doi:10.1890/11-1050.1, 2013.
Klaminder, J., Grip, H., Mörth, C. M. and Laudon, H.: Carbon mineralization and pyrite oxidation in groundwater: Importance for silicate weathering in boreal forest soils and stream base-flow chemistry, Appl. Geochemistry, doi:10.1016/j.apgeochem.2010.12.005, 2011.
Kutscher, L., Mörth, C. M., Porcelli, D., Hirst, C., Maximov, T. C., Petrov, R. E. and Andersson, P. S.: Spatial variation in concentration and sources of organic carbon in the Lena River, Siberia, J. Geophys. Res. Biogeosciences, doi:10.1002/2017JG003858, 2017.
Lammers, R. B., Shiklomanov, A. I., Vörösmarty, C. J., Fekete, B. M. and Peterson, B. J.: Assessment of contemporary Arctic river runoff based on observational discharge records, J. Geophys. Res. Atmos., doi:10.1029/2000JD900444, 2001.
Lange, S.: EartH2Observe, WFDEI and ERA-Interim data Merged and Bias-corrected for ISIMIP (EWEMBI), GFZ Data Serv., doi:10.5880/pik.2016.004, 2016.
Lange, S.: Bias correction of surface downwelling longwave and shortwave radiation for the EWEMBI dataset, Earth Syst. Dyn., doi:10.5194/esd-9-627-2018, 2018.
Lara, R. J., Rachold, V., Kattner, G., Hubberten, H. W., Guggenberger, G., Skoog, A. and Thomas, D. N.: Dissolved organic matter and nutrients in the Lena River, Siberian Arctic: Characteristics and distribution, Mar. Chem., doi:10.1016/S0304-4203(97)00076-5, 1998.
Laudon, H., Buttle, J., Carey, S. K., McDonnell, J., McGuire, K., Seibert, J., Shanley, J., Soulsby, C. and Tetzlaff, D.: Cross-regional prediction of long-term trajectory of stream water DOC response to climate change, Geophys. Res. Lett., doi:10.1029/2012GL053033, 2012.
Lauerwald, R., Hartmann, J., Ludwig, W. and Moosdorf, N.: Assessing the nonconservative fluvial fluxes of dissolved organic carbon in North America, J. Geophys. Res.

Biogeosciences, doi:10.1029/2011JG001820, 2012.
Lauerwald, R., Regnier, P., Camino-Serrano, M., Guenet, B., Guimberteau, M., Ducharne, A., Polcher, J. and Ciais, P.: ORCHILEAK (revision 3875): A new model branch to simulate carbon transfers along the terrestrial-aquatic continuum of the Amazon basin, Geosci. Model Dev., doi:10.5194/gmd-10-3821-2017, 2017.
McGuire, K. J., McDonnell, J. J., Weiler, M., Kendall, C., McGlynn, B. L., Welker, J. M. and Seibert, J.: The role of topography on catchment-scale water residence time, Water Resour. Res., doi:10.1029/2004WR003657, 2005.
Nachtergaele, F. et al.: The harmonized world soil database, FAO, ISRIC,ISSCAS, JRC, doi:3123, 2010.
New, M., Hulme, M. and Jones, P.: Representing twentieth-century space-time climate variability. Part I: Development of a 1961-90 mean monthly terrestrial climatology, J. Clim., 1999.
Qiu, C., Zhu, D., Ciais, P., Guenet, B., Krinner, G., Peng, S., Aurela, M., Bernhofer, C., Brümmer, C., Bret-Harte, S., Chu, H., Chen, J., Desai, A. R., Dušek, J., Euskirchen, E. S., Fortuniak, K., Flanagan, L. B., Friborg, T., Grygoruk, M., Gogo, S., Grünwald, T., Hansen, B. U., Holl, D., Humphreys, E., Hurkuck, M., Kiely, G., Klatt, J., Kutzbach, L., Largeron, C., Laggoun-Défarge, F., Lund, M., Lafleur, P. M., Li, X., Mammarella, I., Merbold, L., Nilsson, M. B., Olejnik, J., Ottosson-Löfvenius, M., Oechel, W., Parmentier, F. J. W., Peichl, M., Pirk, N., Peltola, O., Pawlak, W., Rasse, D., Rinne, J., Shaver, G., Peter Schmid, H., Sottocornola, M., Steinbrecher, R., Sachs, T., Urbaniak, M., Zona, D. and Ziemblinska, K.: ORCHIDEE-PEAT (revision 4596), a model for northern peatland CO2, water, and energy fluxes on daily to annual scales, Geosci. Model Dev., doi:10.5194/gmd-11-497-2018, 2018.
Rawlins, M. A., Fahnestock, M., Frolking, S. and Vörösmarty, C. J.: On the evaluation of snow water equivalent estimates over the terrestrial Arctic drainage basin, in Hydrological Processes., 2007.
Raymond, P. A., McClelland, J. W., Holmes, R. M., Zhulidov, A. V., Mull, K., Peterson, B. J., Striegl, R. G., Aiken, G. R. and Gurtovaya, T. Y.: Flux and age of dissolved organic carbon exported to the Arctic Ocean: A carbon isotopic study of the five largest arctic rivers, Global Biogeochem. Cycles, doi:10.1029/2007GB002934, 2007.
Regnier, P., Friedlingstein, P., Ciais, P., Mackenzie, F. T., Gruber, N., Janssens, I. A., Laruelle, G. G., Lauerwald, R., Luyssaert, S., Andersson, A. J., Arndt, S., Arnosti, C., Borges, A. V., Dale, A. W., Gallego-Sala, A., Goddéris, Y., Goossens, N., Hartmann, J., Heinze, C., Ilyina, T., Joos, F., Larowe, D. E., Leifeld, J., Meysman, F. J. R., Munhoven, G., Raymond, P. A., Spahni, R., Suntharalingam, P. and Thullner, M.: Anthropogenic perturbation of the carbon fluxes from land to ocean, Nat. Geosci., doi:10.1038/ngeo1830, 2013.
Semiletov, I. P., Pipko, I. I., Shakhova, N. E., Dudarev, O. V., Pugach, S. P., Charkin, A. N., Mcroy, C. P., Kosmach, D. and Gustafsson, Ö.: Carbon transport by the Lena River from its headwaters to the Arctic Ocean, with emphasis on fluvial input of terrestrial particulate organic carbon vs. carbon transport by coastal erosion, Biogeosciences, doi:10.5194/bg-8-2407-2011, 2011.
Serikova, S., Pokrovsky, O. S., Ala-Aho, P., Kazantsev, V., Kirpotin, S. N., Kopysov, S. G., Krickov, I. V., Laudon, H., Manasypov, R. M., Shirokova, L. S., Soulsby, C., Tetzlaff, D. and Karlsson, J.: High riverine CO2 emissions at the permafrost boundary of Western Siberia, Nat. Geosci., doi:10.1038/s41561-018-0218-1, 2018.
Shvartsev, S. L.: Geochemistry of fresh groundwater in the main landscape zones of the Earth, Geochemistry Int., doi:10.1134/S0016702908130016, 2008.
Tarnocai, C., Canadell, J. G., Schuur, E. A. G., Kuhry, P., Mazhitova, G. and Zimov, S.: Soil organic carbon pools in the northern circumpolar permafrost retion, Global Biogeochem.

Cycles, doi:Gb2023\n10.1029/2008gb003327, 2009.
Tootchi, A., Jost, A. and Ducharne, A.: Multi-source global wetland maps combining surface water imagery and groundwater constraints, Earth Syst. Sci. Data, doi:10.5194/essd-11-189-2019, 2019.
Vonk, J. E., Mann, P. J., Davydov, S., Davydova, A., Spencer, R. G. M., Schade, J., Sobczak, W. V., Zimov, N., Zimov, S., Bulygina, E., Eglinton, T. I. and Holmes, R. M.: High biolability of ancient permafrost carbon upon thaw, Geophys. Res. Lett., doi:10.1002/grl.50348, 2013.
Vonk, J. E., Tank, S. E., Mann, P. J., Spencer, R. G. M., Treat, C. C., Striegl, R. G., Abbott, B. W. and Wickland, K. P.: Biodegradability of dissolved organic carbon in permafrost soils and aquatic systems: A meta-analysis, Biogeosciences, doi:10.5194/bg-12-6915-2015, 2015a.
Vonk, J. E., Tank, S. E., Bowden, W. B., Laurion, I., Vincent, W. F., Alekseychik, P., Amyot, M., Billet, M. F., Canário, J., Cory, R. M., Deshpande, B. N., Helbig, M., Jammet, M., Karlsson, J., Larouche, J., MacMillan, G., Rautio, M., Walter Anthony, K. M. and Wickland, K. P.: Reviews and Syntheses: Effects of permafrost thaw on arctic aquatic ecosystems, Biogeosciences Discuss., doi:10.5194/bgd-12-10719-2015, 2015b.
Wang, S., Huang, J., Yang, D., Pavlic, G. and Li, J.: Long-term water budget imbalances and error sources for cold region drainage basins, Hydrol. Process., doi:10.1002/hyp.10343, 2015.
Yang, D., Kane, D., Zhang, Z., Legates, D. and Goodison, B.: Bias corrections of long-term (1973-2004) daily precipitation data over the northern regions, Geophys. Res. Lett., doi:10.1029/2005GL024057, 2005.
Ye, B., Yang, D. and Kane, D. L.: Changes in Lena River streamflow hydrology: Human impacts versus natural variations, Water Resour. Res., doi:10.1029/2003WR001991, 2003.
Ye, B., Yang, D., Zhang, Z. and Kane, D. L.: Variation of hydrological regime with permafrost coverage over Lena Basin in Siberia, J. Geophys. Res. Atmos., doi:10.1029/2008JD010537, 2009.
Zhang, X., Hutchings, J. A., Bianchi, T. S., Liu, Y., Arellano, A. R. and Schuur, E. A. G.: Importance of lateral flux and its percolation depth on organic carbon export in Arctic tundra soil: Implications from a soil leaching experiment, J. Geophys. Res. Biogeosciences, doi:10.1002/2016JG003754, 2017.

Tables and Figures:

Table 1: Summary describing of the factorial simulations undertaken to examine the relative drivers of lateral fluxes in our model.

Simulation Name	Abbreviation	Historical Input Data	Input* Held Constant
Control	CTRL	Climate, CO2, Vegetation	None
Constant Climate	CLIM	CO2, Vegetation	Climate
Constant CO2	CO2	Climate, Vegetation	CO2 (Pre-industrial)

*Historically-variable input

Table 2: Mean observed groundwater CO_2 and DOC concentrations for global permafrost regions subdivided by biogeographic province and compiled by Shvartsev (2008) from over 9000 observations.

	Permafrost Groundwater Provinces				
	Swamp	Tundra	Taiga	Average	Average (-Swamp)
CO_2 (mgC L^{-1})	12.3	14	10.8	12.4	12.4
DOC (mgC L^{-1})	17.6	10.1	9.3	12.3	9.7

Table 3: Summary of the average carbon reactivity types comprising the hydrological inputs to rivers and streams (runoff, drainage and floodplain inputs), and within the rivers and streams themselves, subdivided between the 'North' and 'South' of the Lena basin (greater or less than 63N, respectively).

Hydrological Source	**Model Carbon Reactivity Pool**	**North**	**South**
Runoff Input	Refractory	81%	83%
	Labile	19%	17%
Drainage Input	Refractory	96%	94%
	Labile	4%	6%
Flood Input	Refractory	36%	37%
	Labile	64%	63%
Streams	Refractory	91%	89%
	Labile	9%	11%
Rivers	Refractory	92%	90%
	Labile	8%	10%

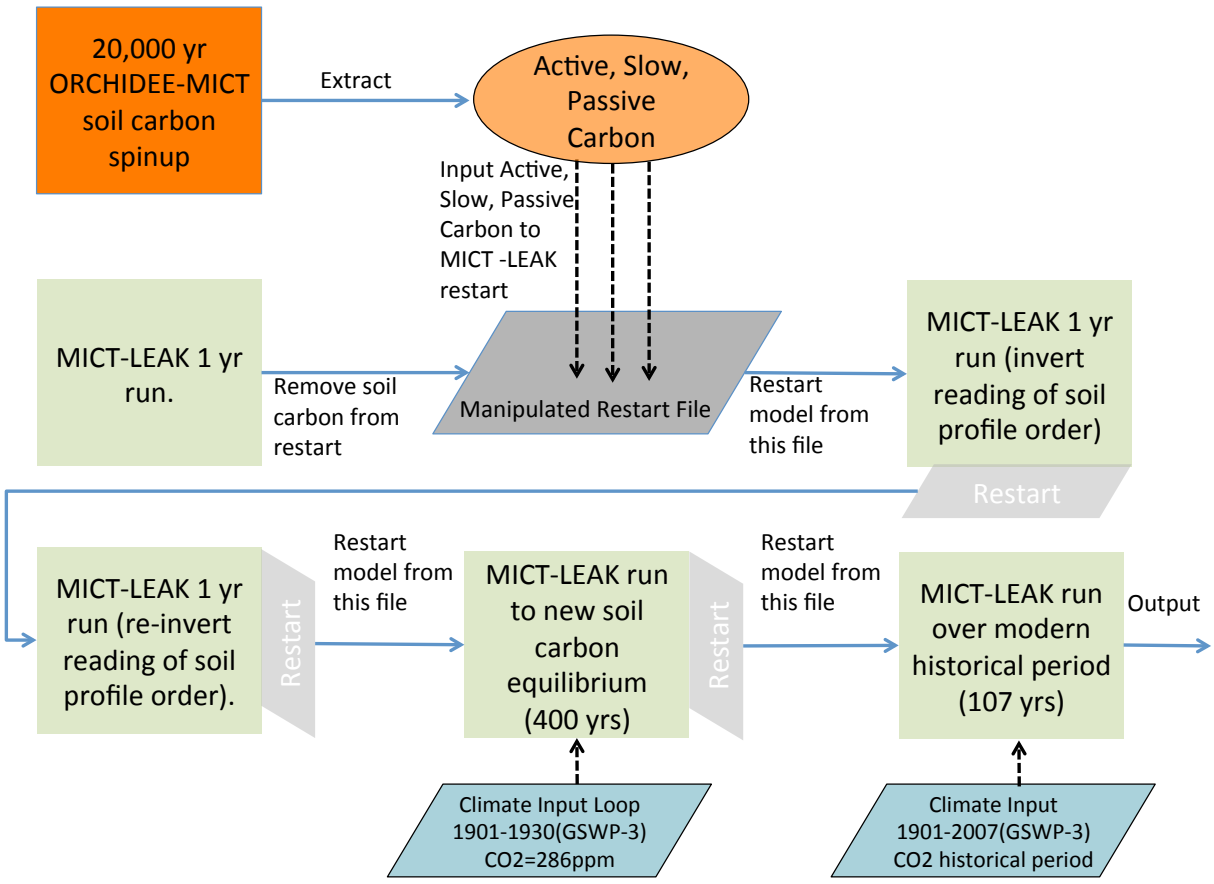

Figure 1: Flow diagram illustrating the step-wise stages required to set up the model, up to and including the historical period. The two stages that refer to the inverted reading of restart soil profile order point to the fact that the restart inputs from ORCHIDEE-MICT are read by our model in inverse order, so that one year must be run in which an activated flag reads it properly, before the reading of soil profile restarts is re-inverted for all subsequent years.

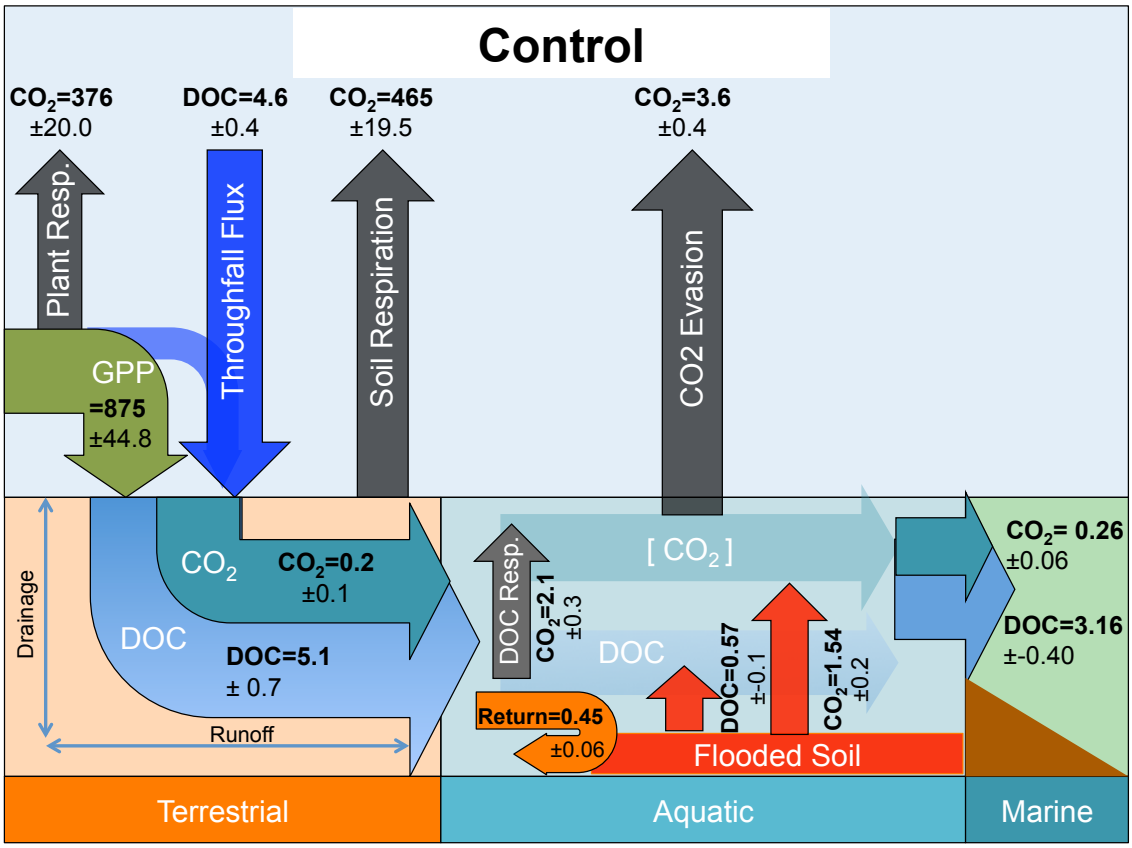

Figure 2: Schematic diagrams detailing the major yearly carbon flux outputs (TgC yr^{-1}) from the Control simulation averaged over the period 1998-2007 as they are transformed and transported across the land-aquatic continuum.

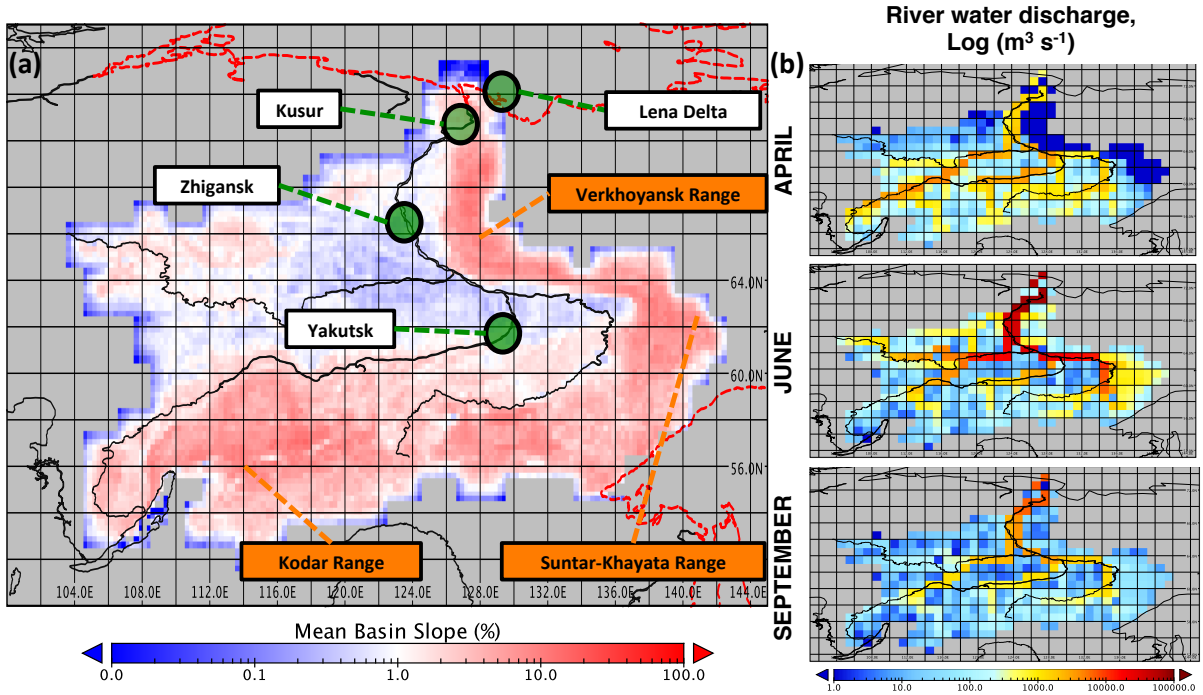

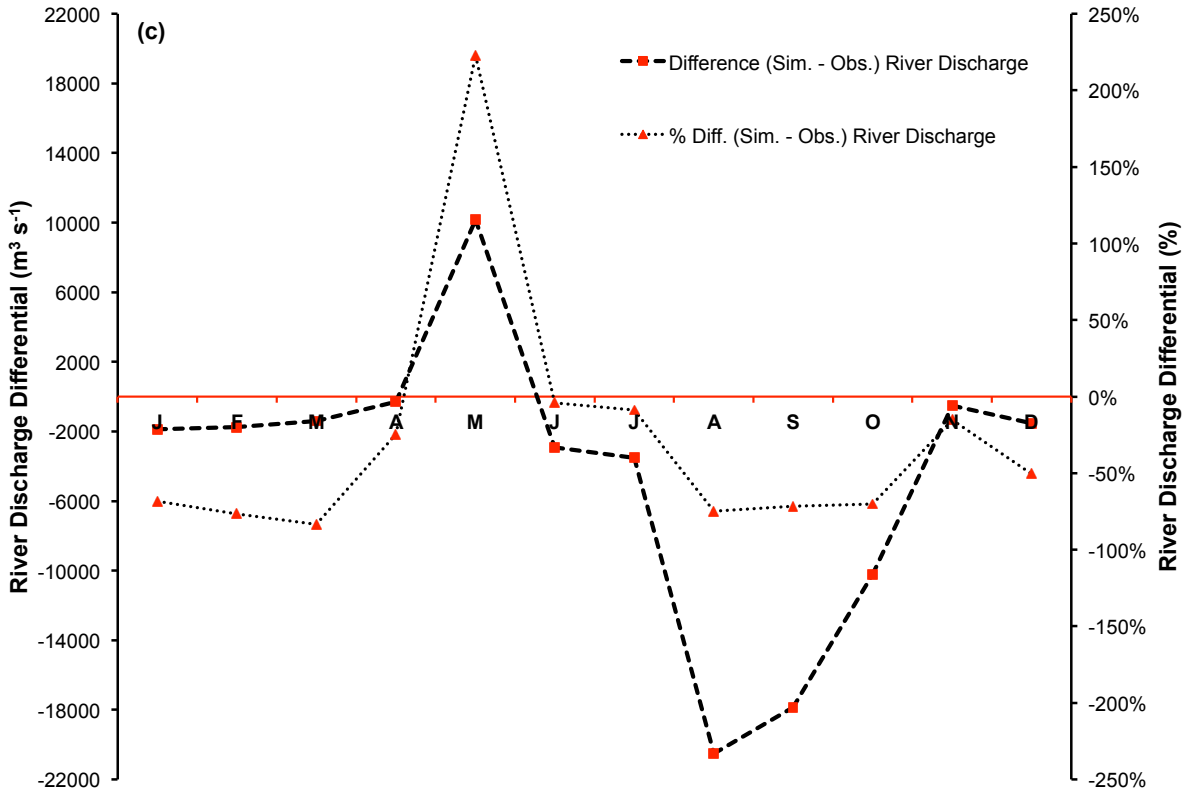

1248
1249

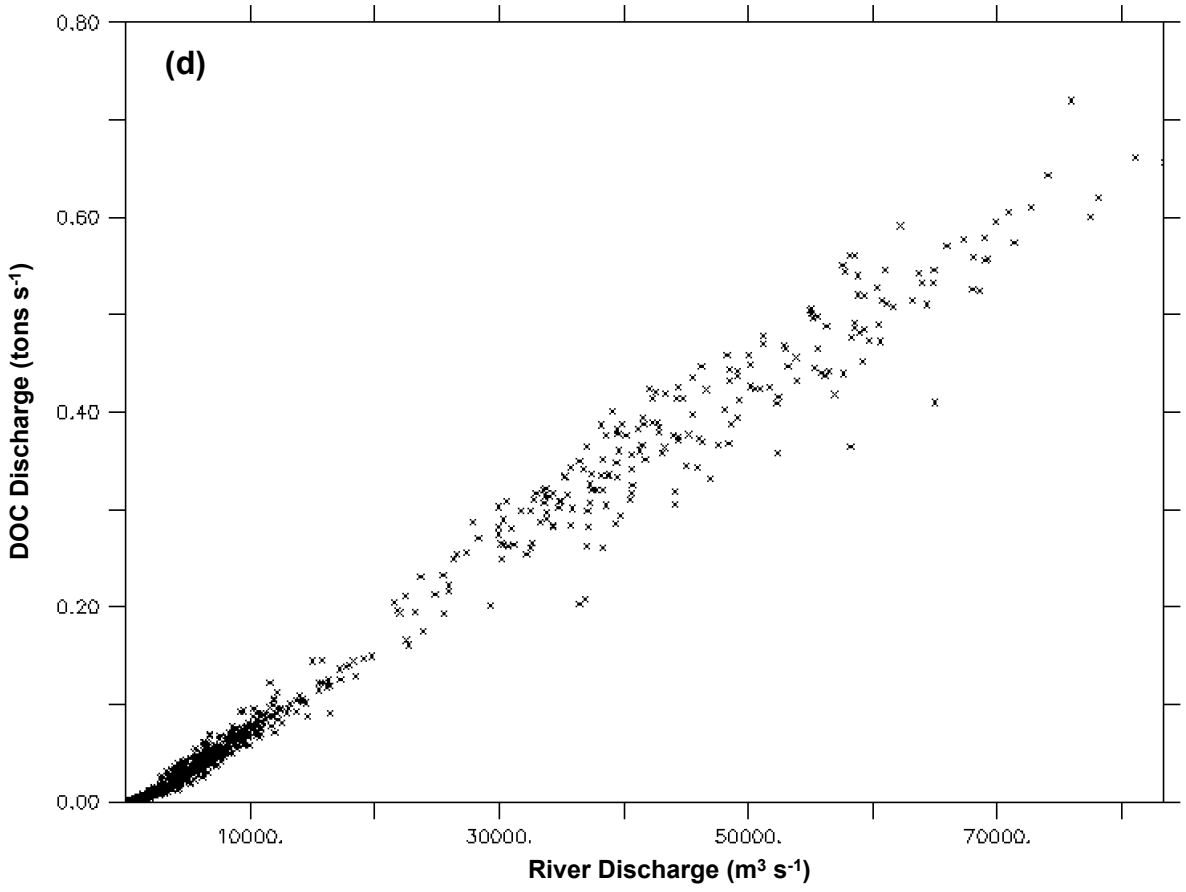

1250

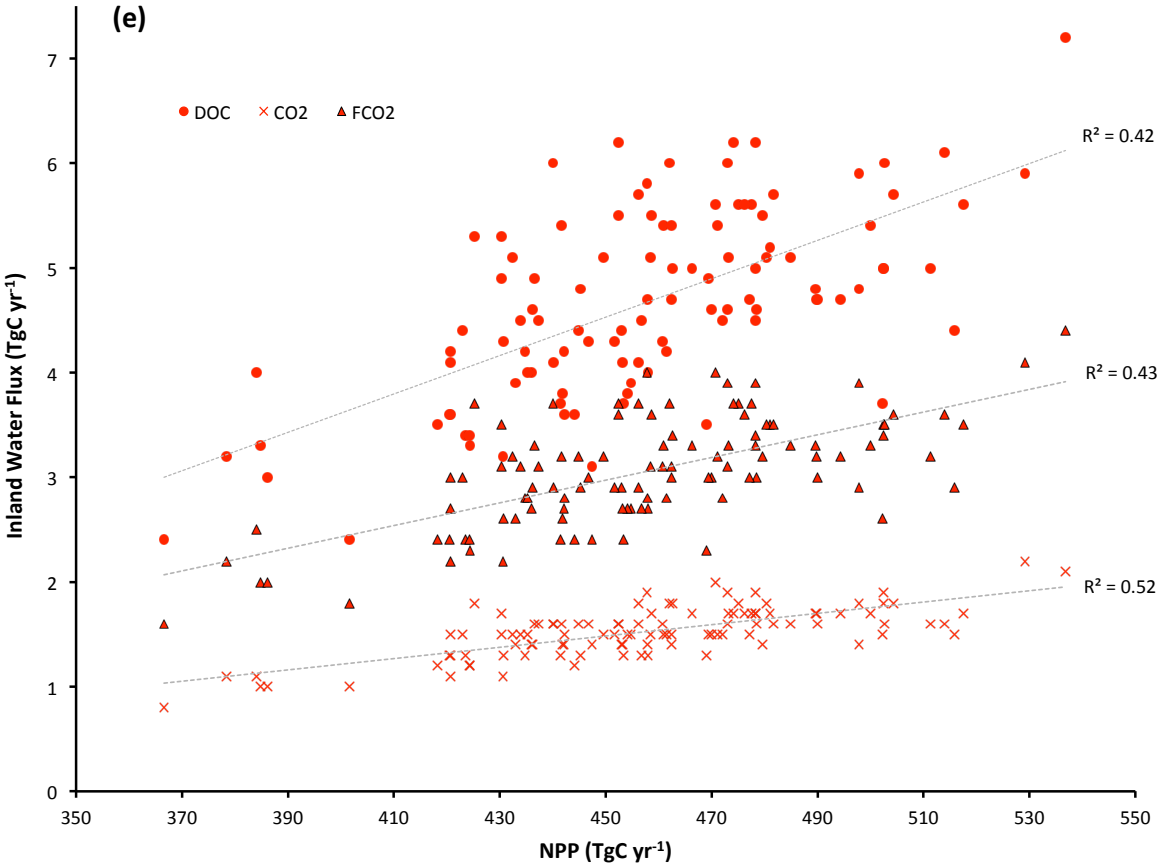

Figure 3: Map of the Lena **(a)** with the scale bar showing the mean grid cell topographic slope from the simulation, and the black line the satellite-derived overlay of the river main stem and sub-basins. Mountain ranges of the Lena basin are shown in orange. Green circles denote the outflow gridcell (Kusur) from which our simulation outflow data are derived, as well as the Zhigansk site, from which out evaluation against data from Raymond et al. (2007) are assessed. The regional capital (Yakutsk) is also included for geographic reference. Coastal outline and inland water bodies are shown as dashed red and solid black lines, respectively. **(b)** Maps of river water discharge (log(m^3 s^{-1})) in April, June and September, averaged over 1998-2007. **(c)** The mean monthly river discharge differential between observed discharge for the Lena (Ye et al., 2009) and simulated discharge averaged over 1998-2007, in absolute (m^3 s^{-1}) and percentage terms. **(d)** Regression of simulated monthly DOC discharge versus simulated river discharge at the river mouth (Kusur) over the entire simulation period (1901-2007). **(e)** Summed yearly lateral flux versus NPP values for DOC discharge, CO_2 discharge and CO_2 evasion (FCO_2) over the entire simulation period, with linear regression lines shown.

(a)

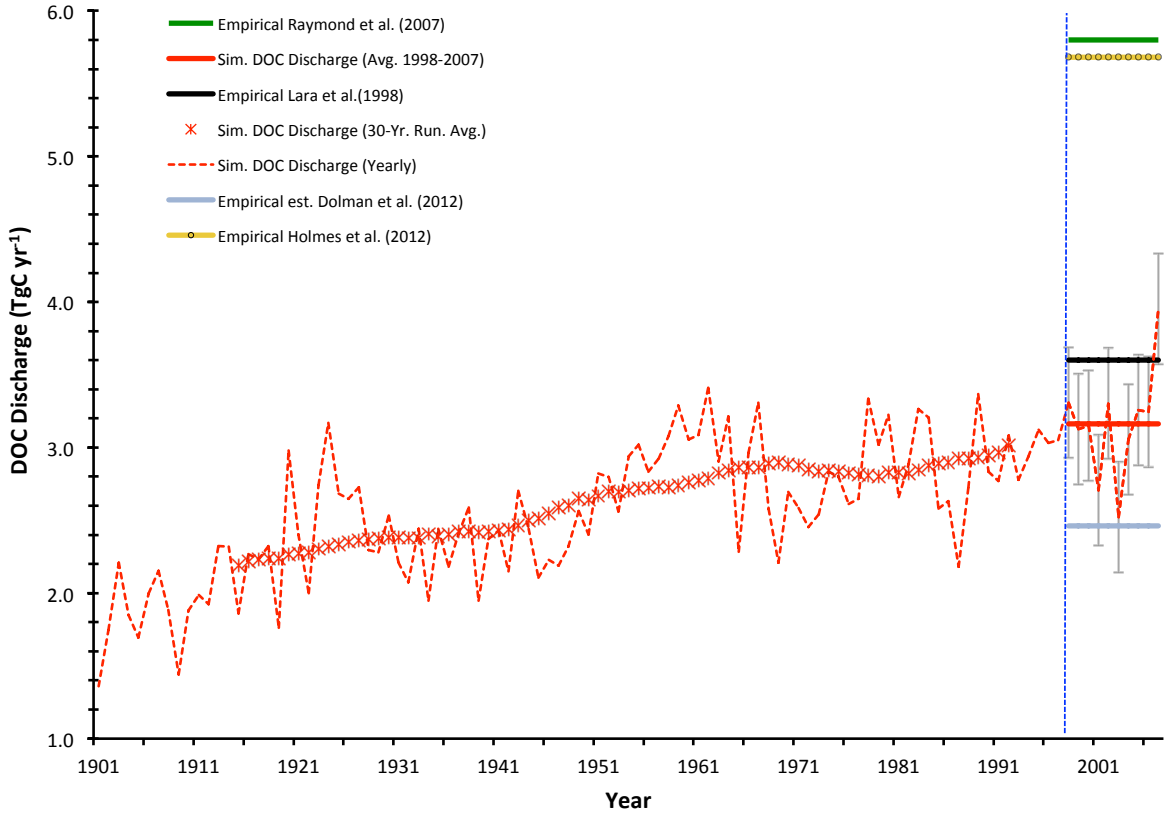
Empirical Raymond et al. (2007)
Sim. DOC Discharge (Avg. 1998-2007)
Empirical Lara et al.(1998)
Sim. DOC Discharge (30-Yr. Run. Avg.)
Sim. DOC Discharge (Yearly)
Empirical est. Dolman et al. (2012)
Empirical Holmes et al. (2012)
DOC Discharge (TgC yr-1)
6.0
5.0
4.0
3.0
2.0
1.0
1901
1911
1921
1931
1941
1951
1961
1971
1981
1991
2001
Year

(b)

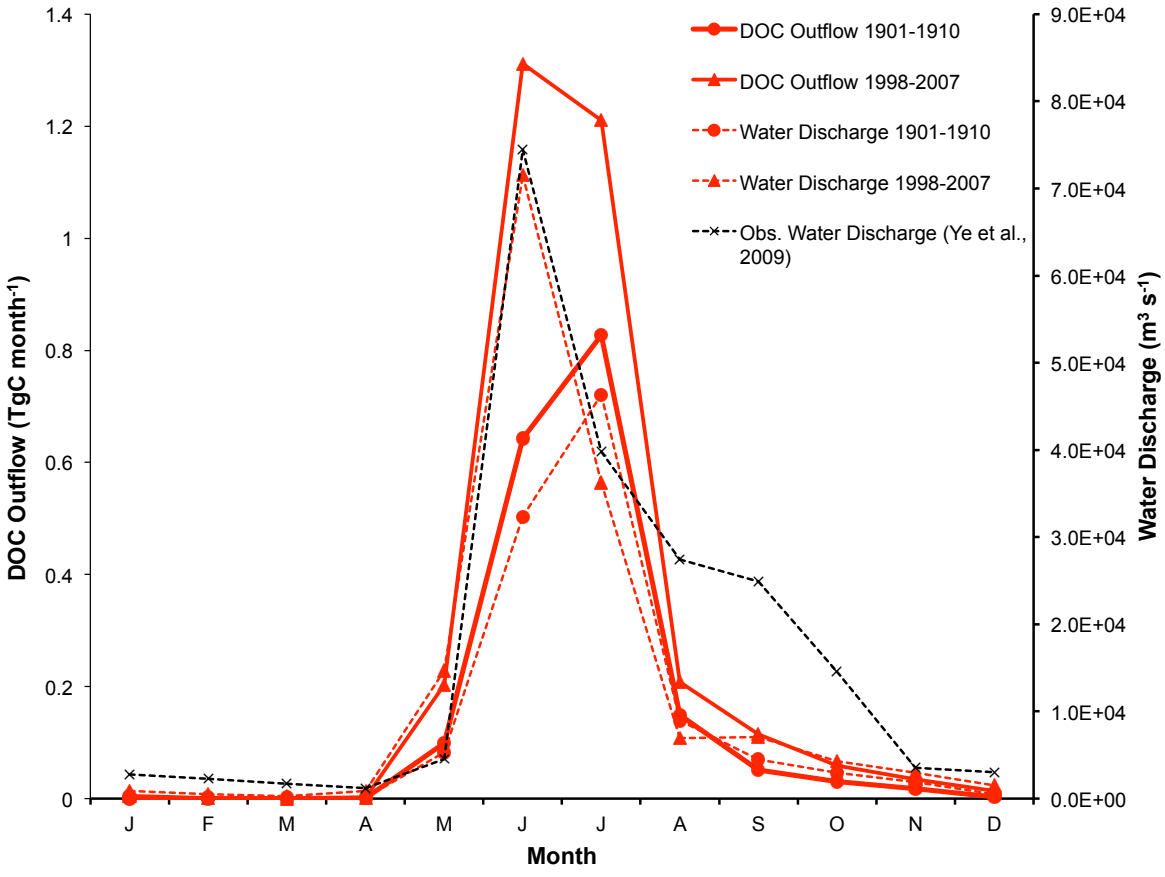
DOC Outflow 1901-1910
DOC Outflow 1998-2007
Water Discharge 1901-1910
Water Discharge 1998-2007
Obs. Water Discharge (Ye et al., 2009)
DOC Outflow (TgC month-1)
Water Discharge (m3 s-1)
1.4
1.2
1
0.8
0.6
0.4
0.2
0
9.0E+04
8.0E+04
7.0E+04
6.0E+04
5.0E+04
4.0E+04
3.0E+04
2.0E+04
1.0E+04
0.0E+00
J
F
M
A
M
J
J
A
S
O
N
D
Month

(c)

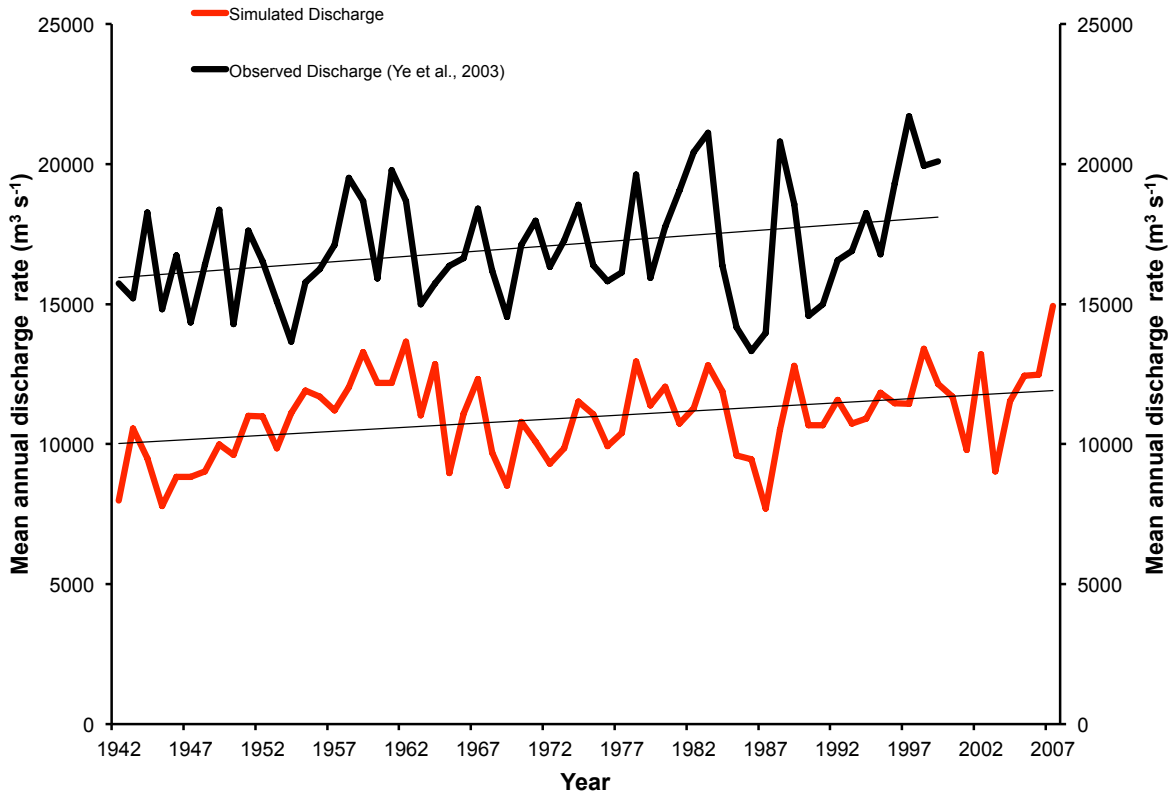
Simulated Discharge
Observed Discharge (Ye et al., 2003)
Mean annual discharge rate (m³ s⁻¹)
Mean annual discharge rate (m³ s⁻¹)
25000
20000
15000
10000
5000
0
1942
1947
1952
1957
1962
1967
1972
1977
1982
1987
1992
1997
2002
2007
Year

(d)

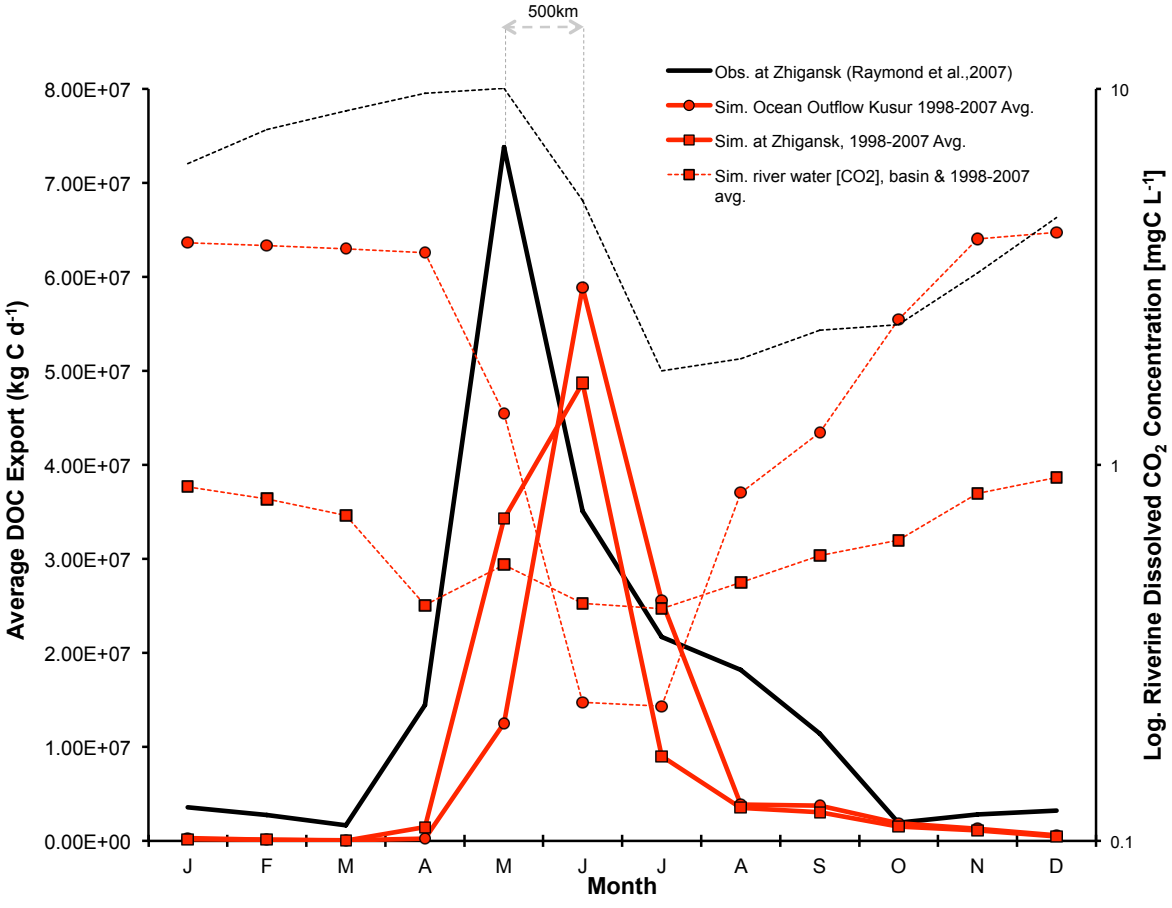
500km
Obs. at Zhigansk (Raymond et al.,2007)
Sim. Ocean Outflow Kusur 1998-2007 Avg.
Sim. at Zhigansk, 1998-2007 Avg.
Sim. river water [CO2], basin & 1998-2007 avg.
Average DOC Export (kg C d⁻¹)
Log. Riverine Dissolved CO2 Concentration [mgC L⁻¹]
8.00E+07
7.00E+07
6.00E+07
5.00E+07
4.00E+07
3.00E+07
2.00E+07
1.00E+07
0.00E+00
10
1
0.1
J
F
M
A
M
J
J
A
S
O
N
D
Month

Figure 4: **(a)** Yearly DOC discharged from the Lena river into the Laptev sea is shown here in tC yr^{-1}, over the entire simulation period (dashed red line), with the smoothed, 30-year running mean shown in asterisk. Observation based estimates for DOC discharge from Lara et al. (1998), Raymond et al. (2007), Dolman et al. (2012) and Holmes et al. (2012) are shown by the horizontal black, green triangle, blue diamond and yellow circle line colours and symbols, respectively, and are to be compared against the simulated mean over the last decade of simulation (1998-2007, horizontal red line), with error bars added in grey displaying the standard deviation of simulated values over that period. **(b)** Average monthly DOC discharge (solid red, tC $month^{-1}$) and water discharge (dashed red, m^3 s^{-1}) to the Laptev Sea over the period averaged for 1901-1910 (circles) and 1997-2007 (squares) are compared, with modern maxima closely tracking observed values. Observed water discharge over 1936-2000 from R-ArcticNet v.4 (Lammers et al., 2001) and published in Ye et al. (2009) are shown by the dashed black line. **(c)** Observed versus simulated mean annual water discharge from the Lena river, where observations are taken from (Ye et al., 2003) **(d)** Observed (black) and simulated (red) seasonal DOC fluxes (solid lines) and CO_2 discharge concentrations (dashed lines). Observed DOC discharge as published in Raymond et al. (2007) from 2004-2005 observations at Zhigansk, a site ~500km upstream of the Lena delta. This is plotted against simulated discharge for: (i) the Lena delta at Kusur (red circles) and (ii) the approximate grid pixel corresponding to the Zhigansk site (red squares) averaged over 1998-2008. Observed CO_2 discharge from a downstream site (Cauwet & Sidorov, 1996; dashed black), and simulated from the outflow site (dashed circle) and the basin average (dashed square) are shown on the log-scale right-hand axis for 1998-2008.

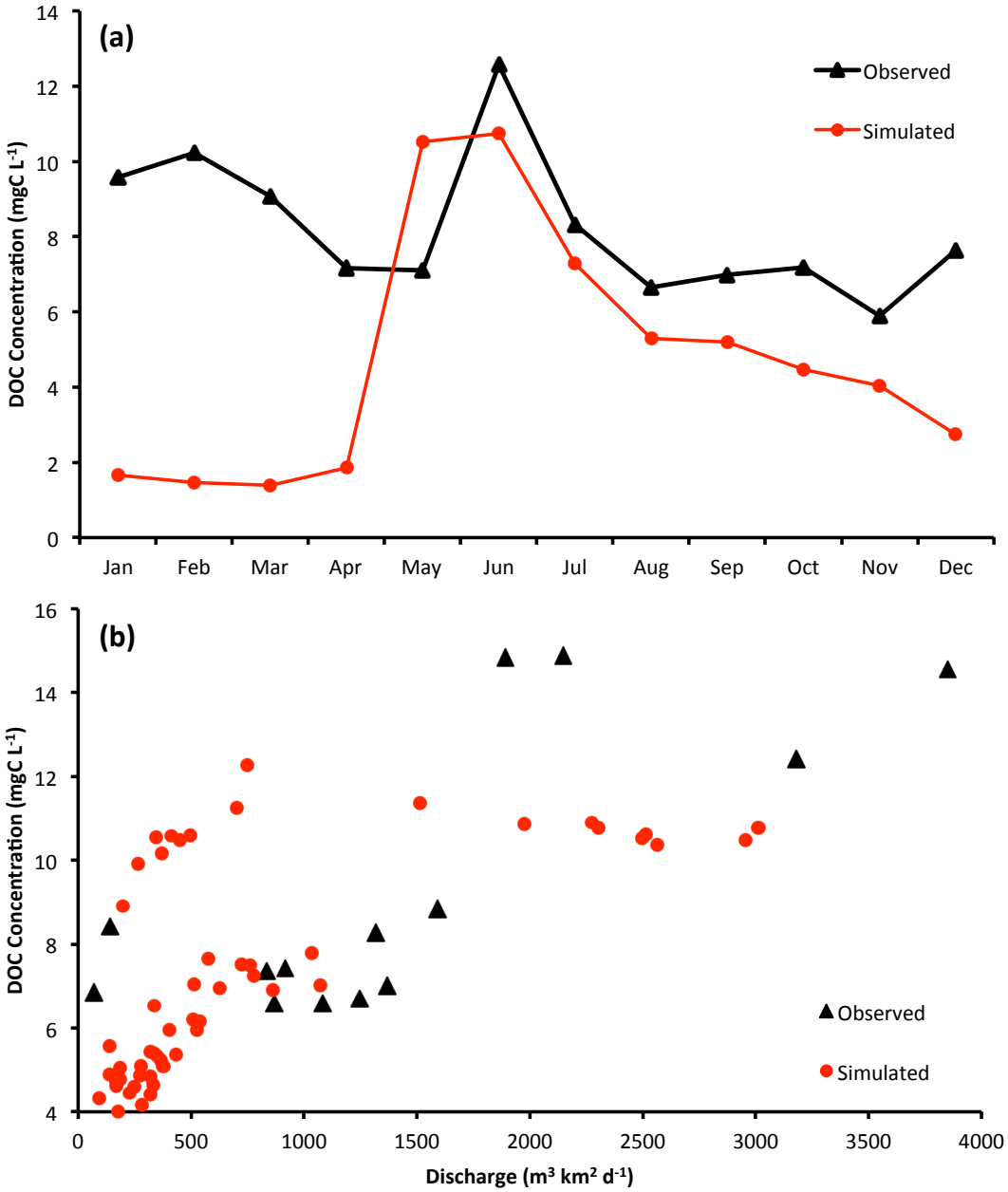

Figure 5: (a) Simulated and observed (Arctic-GRO/Holmes et al., 2012) DOC concentration seasonality for the Lena basin over the period 1999-2007. **(b)** Plots of DOC concentration versus river discharge as in observations (Raymond et al., 2007) and simulations, where simulations data points are monthly averages taken over the period 1999-2007

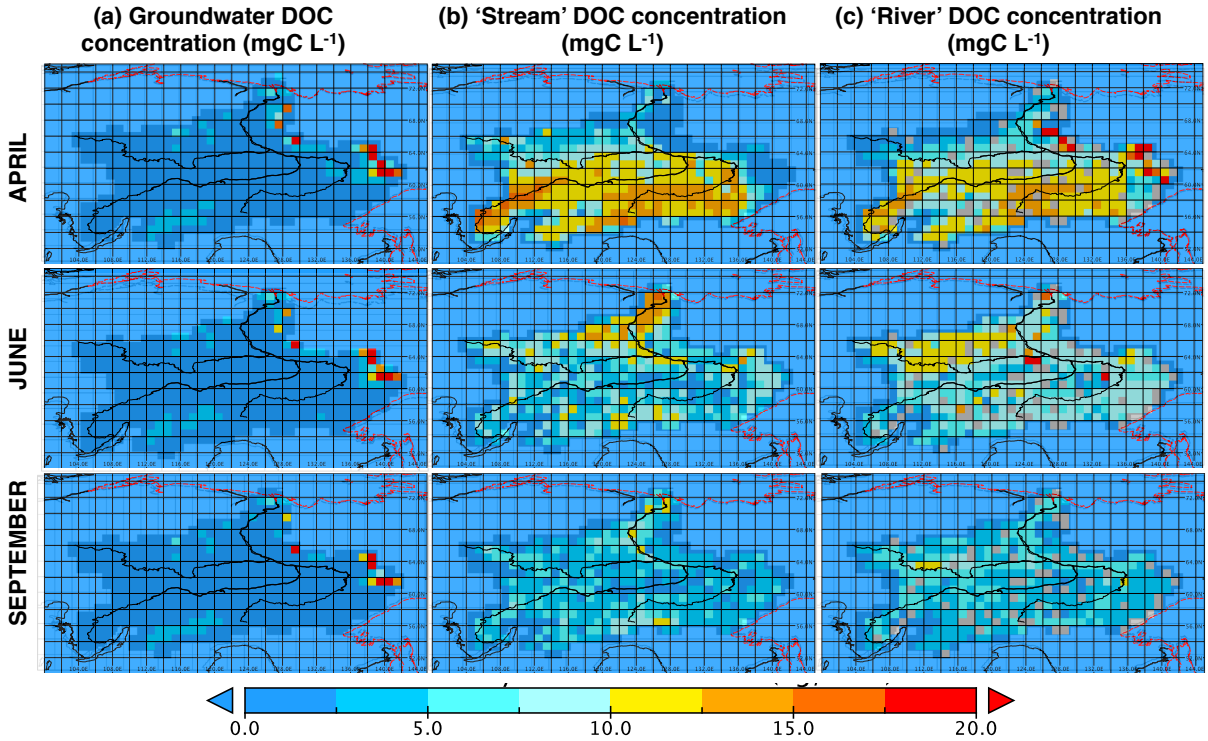

Figure 6: Maps of **(a)** DOC concentrations (mgC L^{-1}) in groundwater ('slow' water pool), **(b)** stream water pool, **(c)** river water pool in April, June and September (first to third rows, respectively), averaged over the period 1998-2007. The coastal boundary and a water body overlay have been applied to the graphic in red and black, respectively, and the same scale applies to all diagrams. All maps have the Lena basin area shaded in the background.

(a)

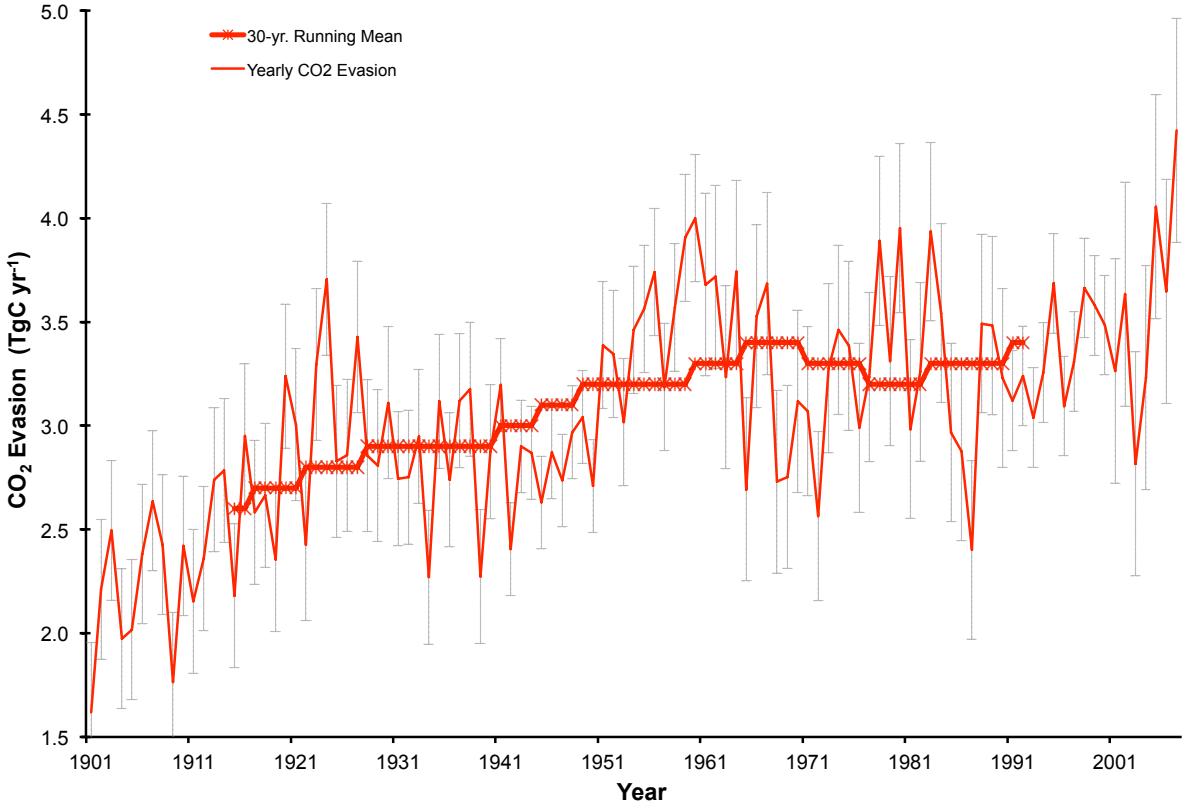
30-yr. Running Mean
Yearly CO2 Evasion
CO_2 Evasion (TgC yr^{-1})
5.0
4.5
4.0
3.5
3.0
2.5
2.0
1.5
1901
1911
1921
1931
1941
1951
1961
1971
1981
1991
2001
Year

(b)

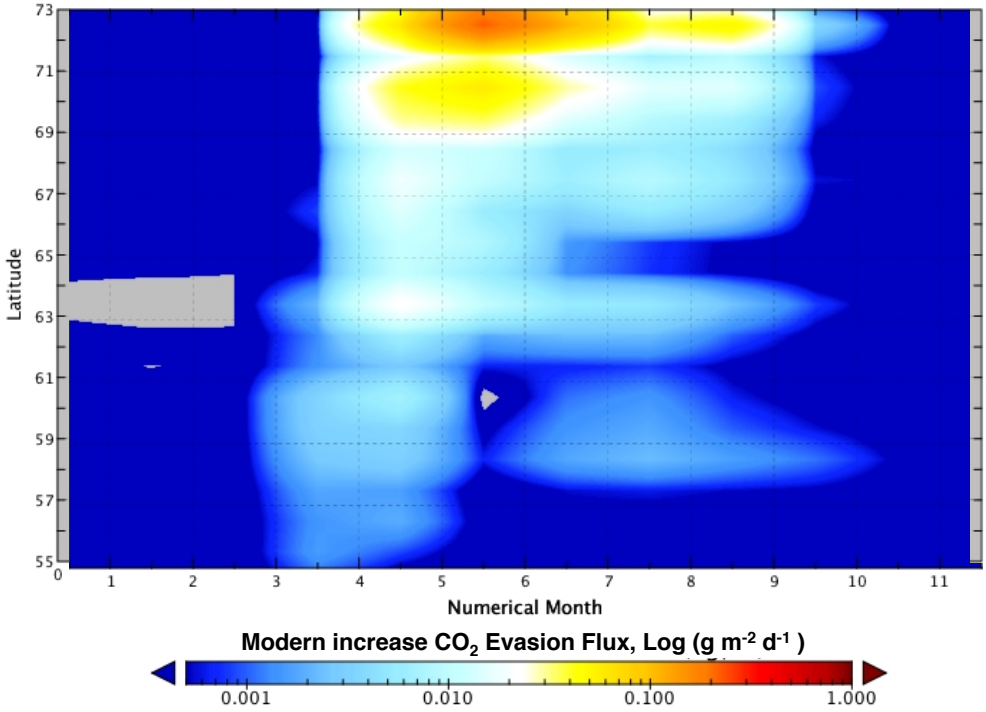
Latitude
73
71
69
67
65
63
61
59
57
55
0
1
2
3
4
5
6
7
8
9
10
11
Numerical Month
Modern increase CO_2 Evasion Flux, Log (g m^{-2} d^{-1})
0.001
0.010
0.100
1.000

(c)

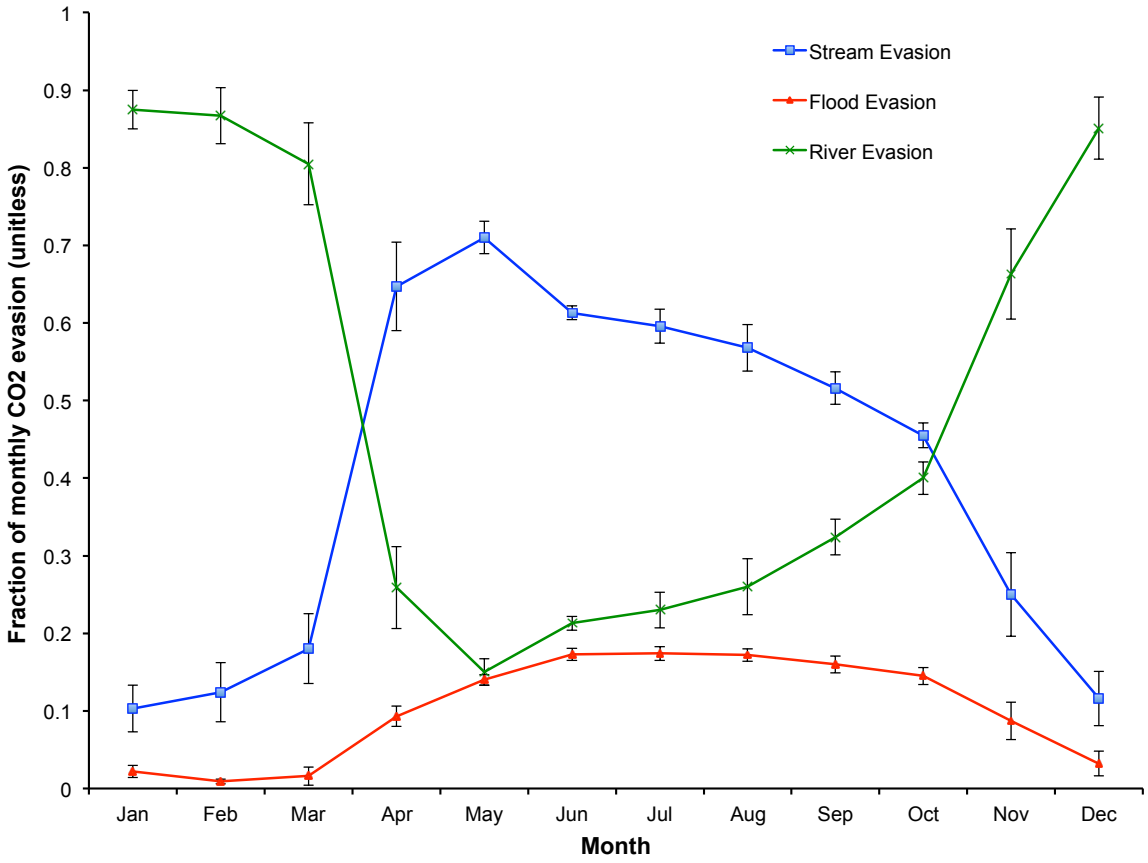
Stream Evasion
Flood Evasion
River Evasion
Fraction of monthly CO2 evasion (unitless)
Month
Jan
Feb
Mar
Apr
May
Jun
Jul
Aug
Sep
Oct
Nov
Dec

(d)

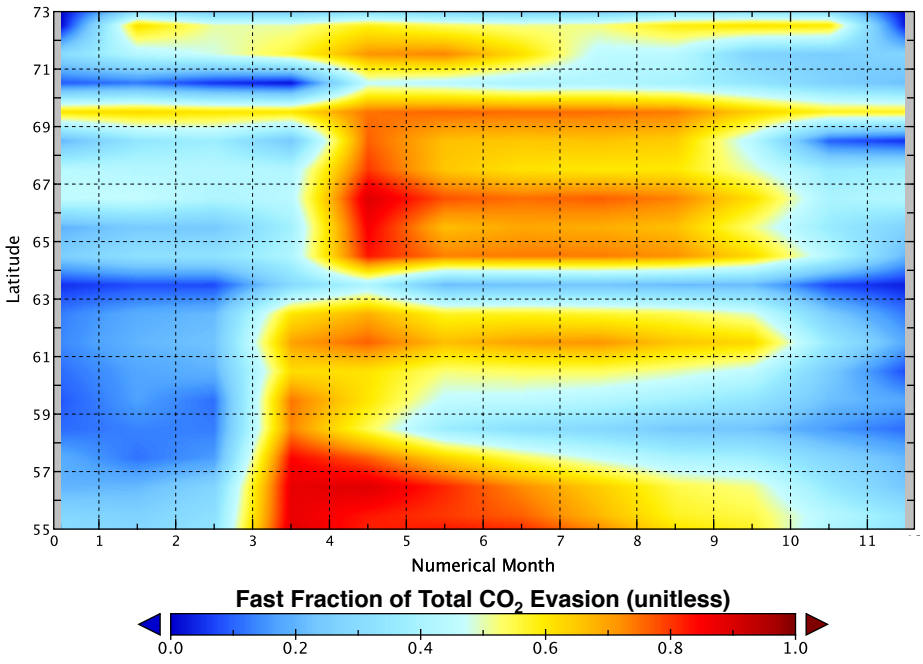
Latitude
Numerical Month
Fast Fraction of Total CO_2 Evasion (unitless)

(e)

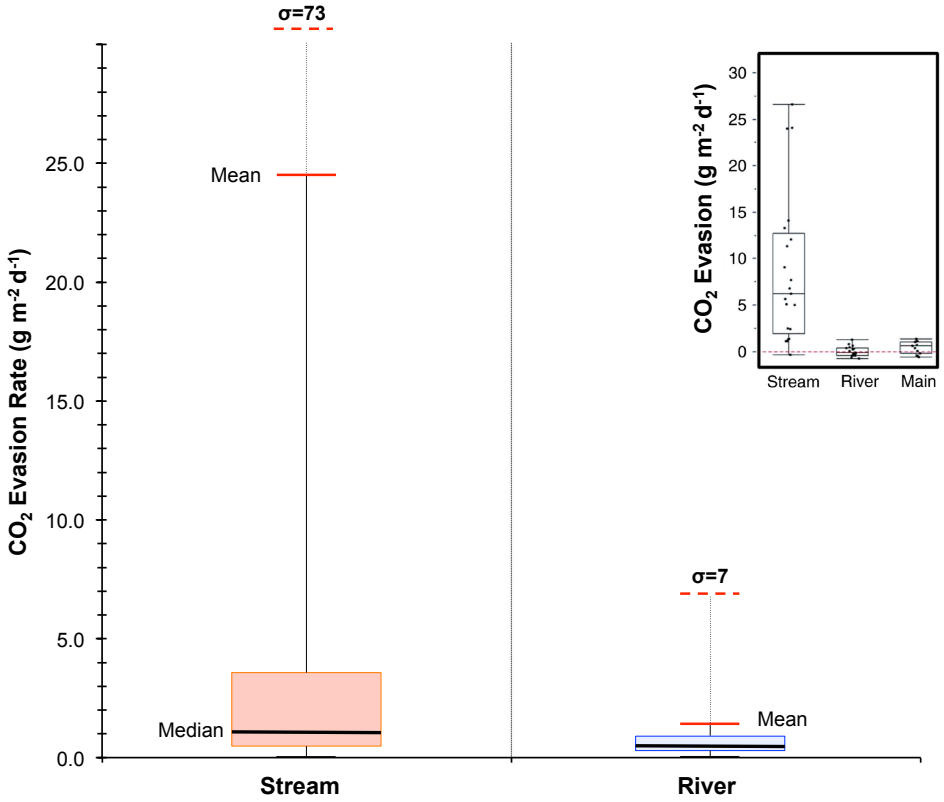

Figure 7: CO_2 evasion from stream, river, flood reservoirs. **(a)** Timeseries of total yearly CO_2 evasion (tC yr^{-1}) summed over the three hydrological pools (red line) with the 30-year running mean of the same variable overlain in thick red (asterisk). Error bars give the standard deviation of each decade (e.g. 1901-1910) for each data point in that decade. **(b)** Log-scale Hovmöller diagram plotting the longitudinally-averaged difference (increase) in total CO_2 evaded from the Lena River basin between the average of the periods 1998-2007 and 1901-1910, over each montly timestep, in (log) gC m^{-2} d^{-1}. Thus as the river drains northward the month-on-month difference in water-body CO_2 flux, between the beginning and end of the 20th Century is shown; **(c)** The fraction of total CO_2 evasion emitted from each of the hydrological pools for the average of each month over the period 1998-2007 is shown for river, flood and stream pools (blue, green and red lines, respectively), with error bars depicting the standard deviation of data values for each month displayed. **(d)** Hovmöller diagram showing the monthly evolution of the stream pool fraction (range 0-1) per month and per latitudinal band, averaged over the period 1998-2007. **(e)** Boxplot for approximate (see text) simulated CO_2 evasion (gC m^{-2} d^{-1}) from the streamwater reservoir and river water reservoir averaged over 1998-2007. Coloured boxes denote the first and third quartiles of the data range, internal black bars the median. Whiskers give the mean (solid red bar) and standard deviation (dashed red bar) of the respective data. Empirical data on these quantities using the same scale for rivers, streams and mainstem of the Kolyma river from Denfeld et al., 2013 are shown inset.

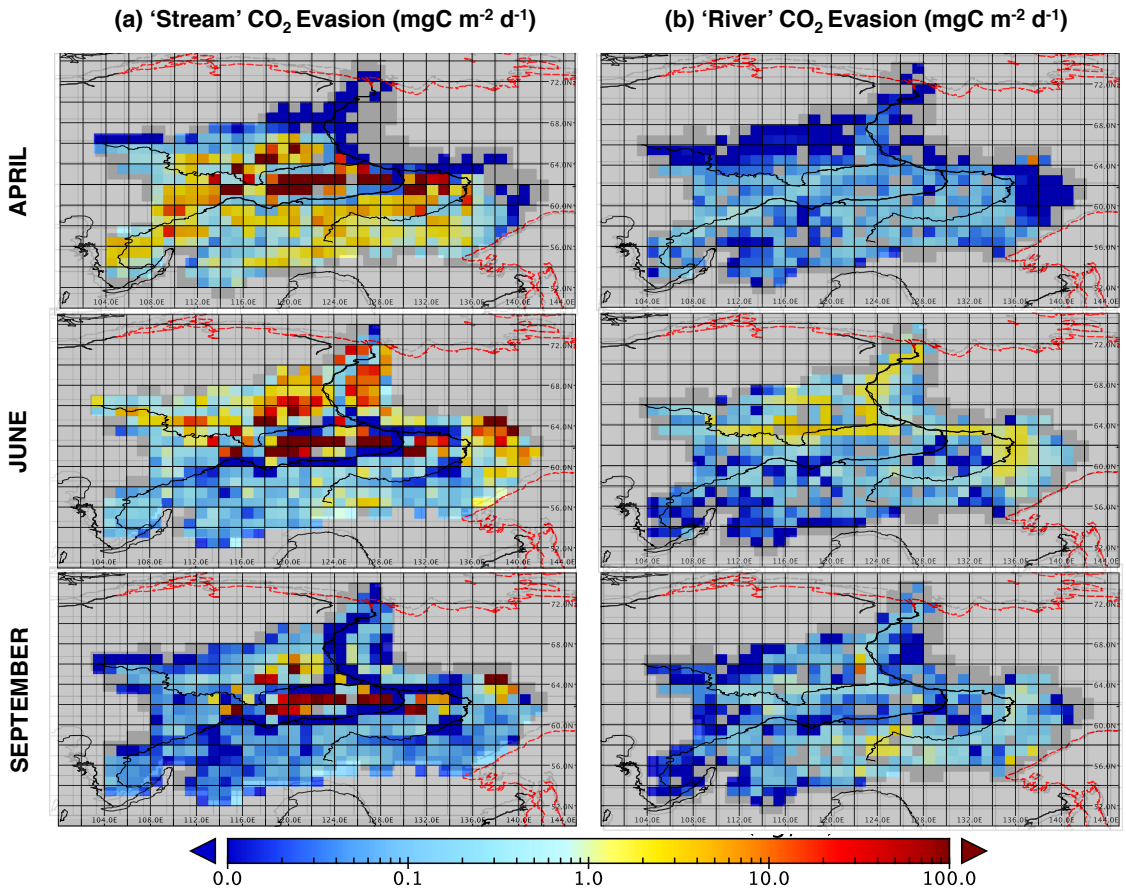

Figure 8: Maps of CO_2 evasion from the surface of the two fluvial hydrological pools in the model, (a) streams and (b) rivers in April, June and September. All maps use the same (log) scale in units of (mgC m^{-2} d^{-1}).

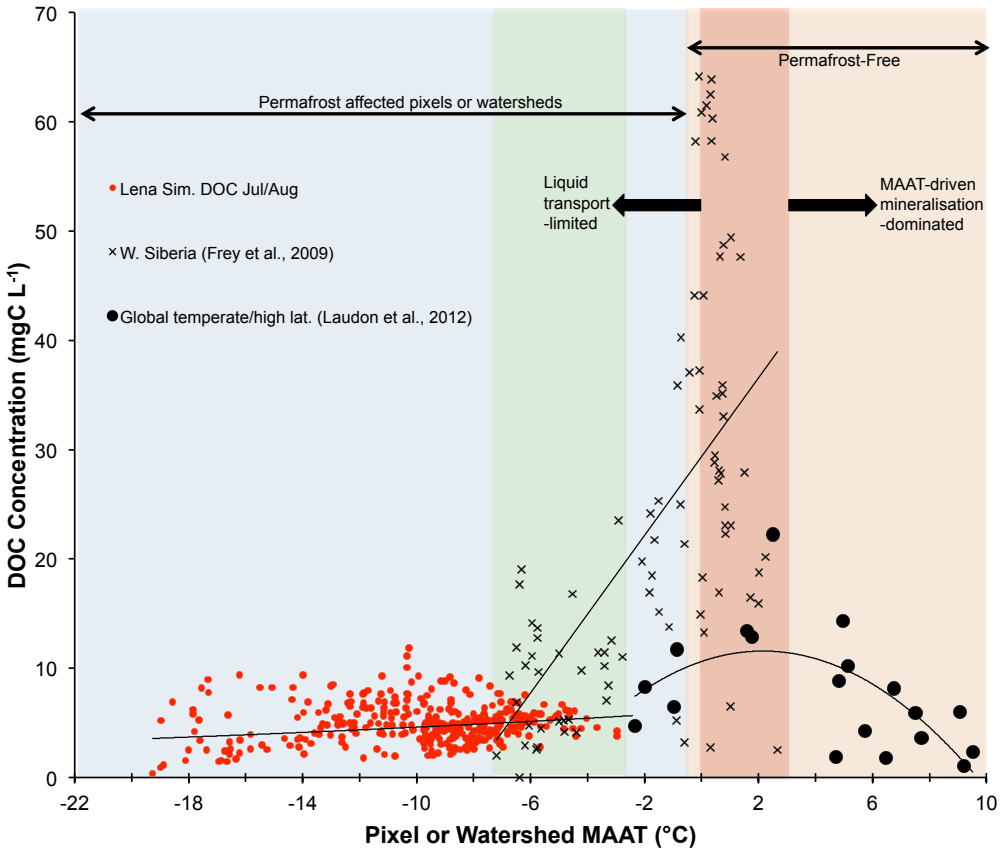

Figure 9: Mean summertime DOC concentrations (mgC L^{-1}) plotted against mean annual air temperature (MAAT, °Celsius) for simulated pixels over the Lena river basin (red circles), and observations for largely peat-influenced areas in western Siberia as reported in Frey et al., 2009 (black crosses), and observations from a global non-peat temperate and high latitude meta-analysis (black circles) reported in Laudon et al. (2012). The blue region represents permafrost-affected areas, while the orange region represents permafrost-free areas. The green region bounds the area of overlap in MAAT between the observed and simulated datasets. The dark red shaded area corresponds to the MAAT 'zone of optimality' for DOC production and transport proposed by Laudon et al. (2012). Regression curves of DOC against MAAT for each of the separate datasets are shown for each individual dataset.

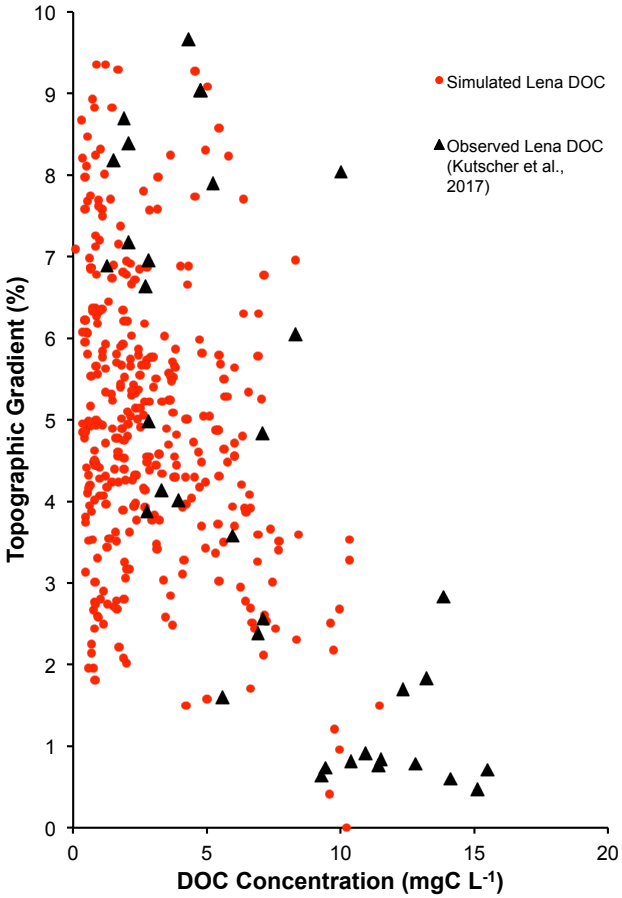

Figure 10: Variation of DOC concentrations versus topographic slope in Kutscher et al., 2017 (black triangles) and (red dots) as simulated and averaged for the summer months (JJA) over 1998-2007; observed values were measured during June and July 2012-2013.

(a)

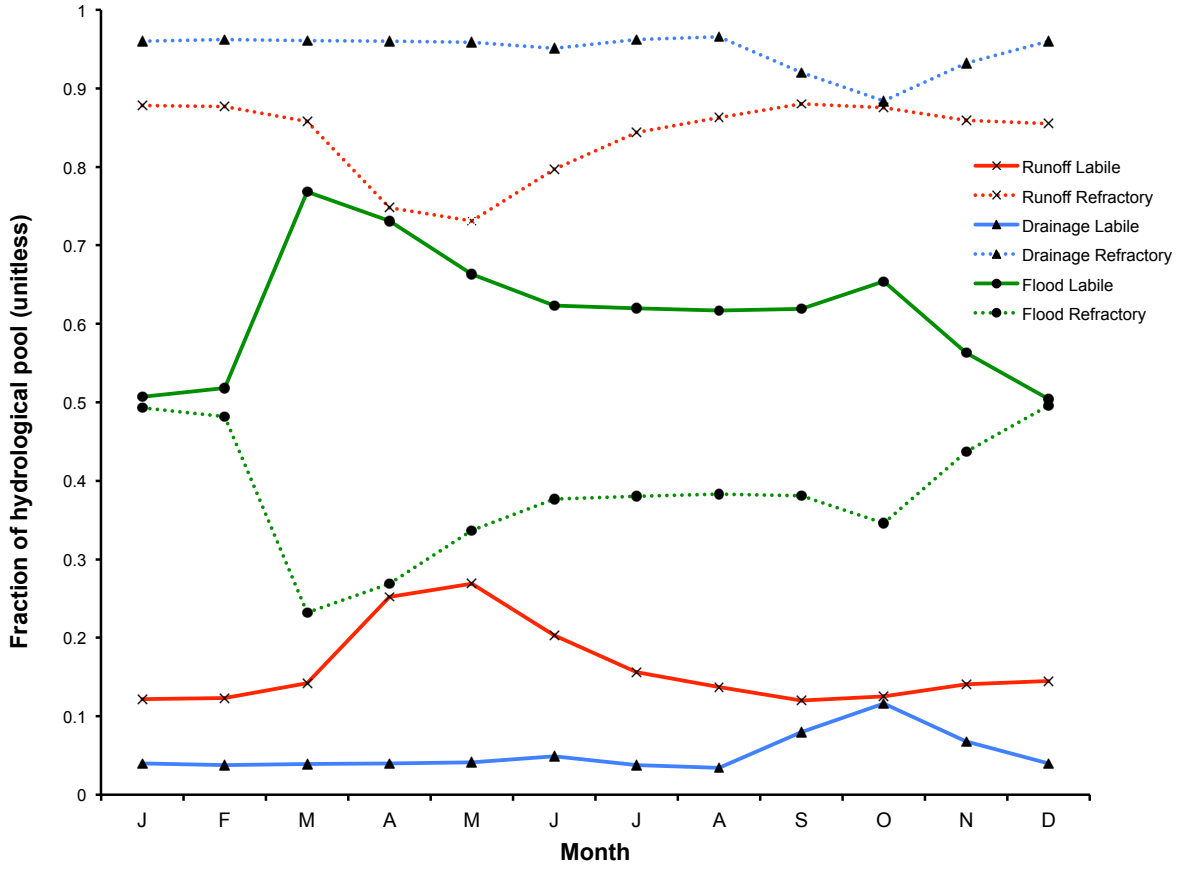

Figure 11: The mean monthly fraction of each hydrological pool's (runoff, drainage, floodplains) carbon reactivity constituents (labile and refractory) averaged across the simulation area over 1998-2008.

1382 **(a)**

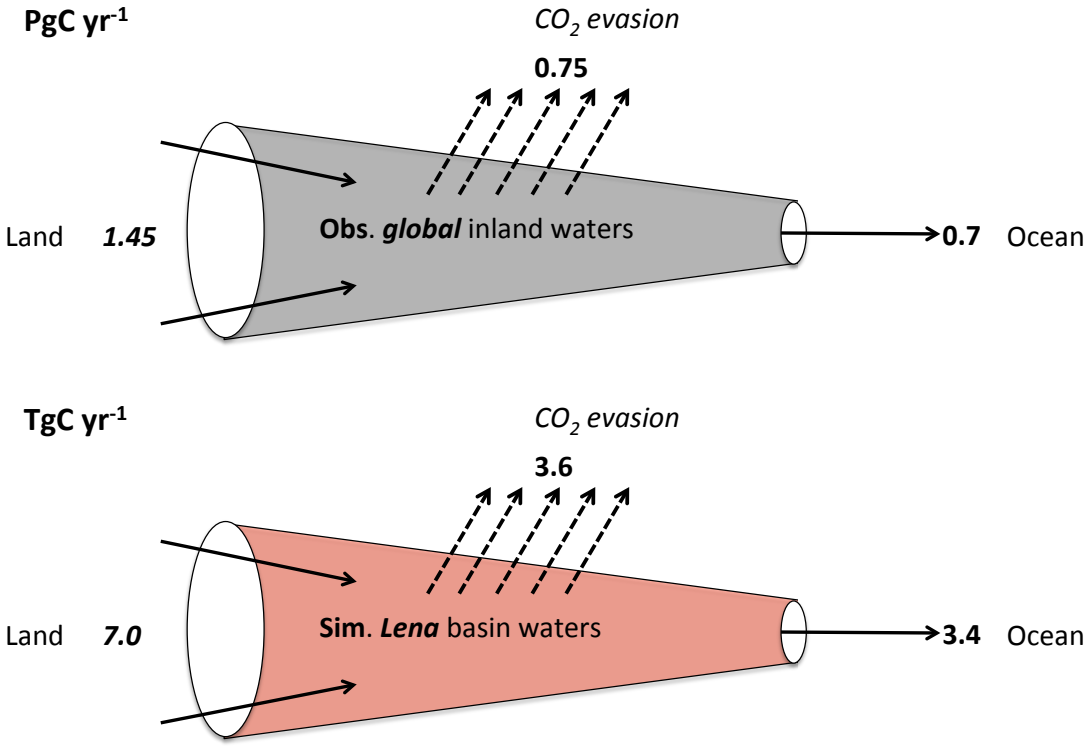

1383
1384 **(b)**

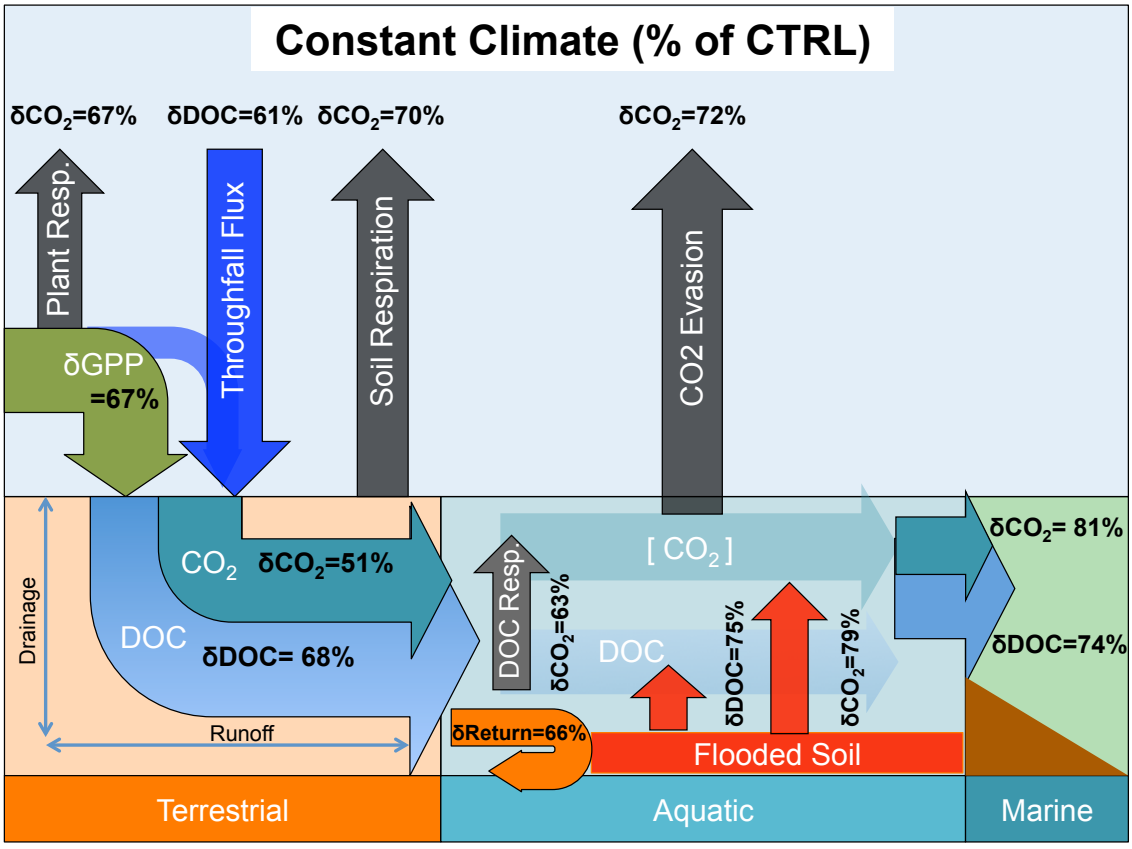

1385
1386 **(c)**

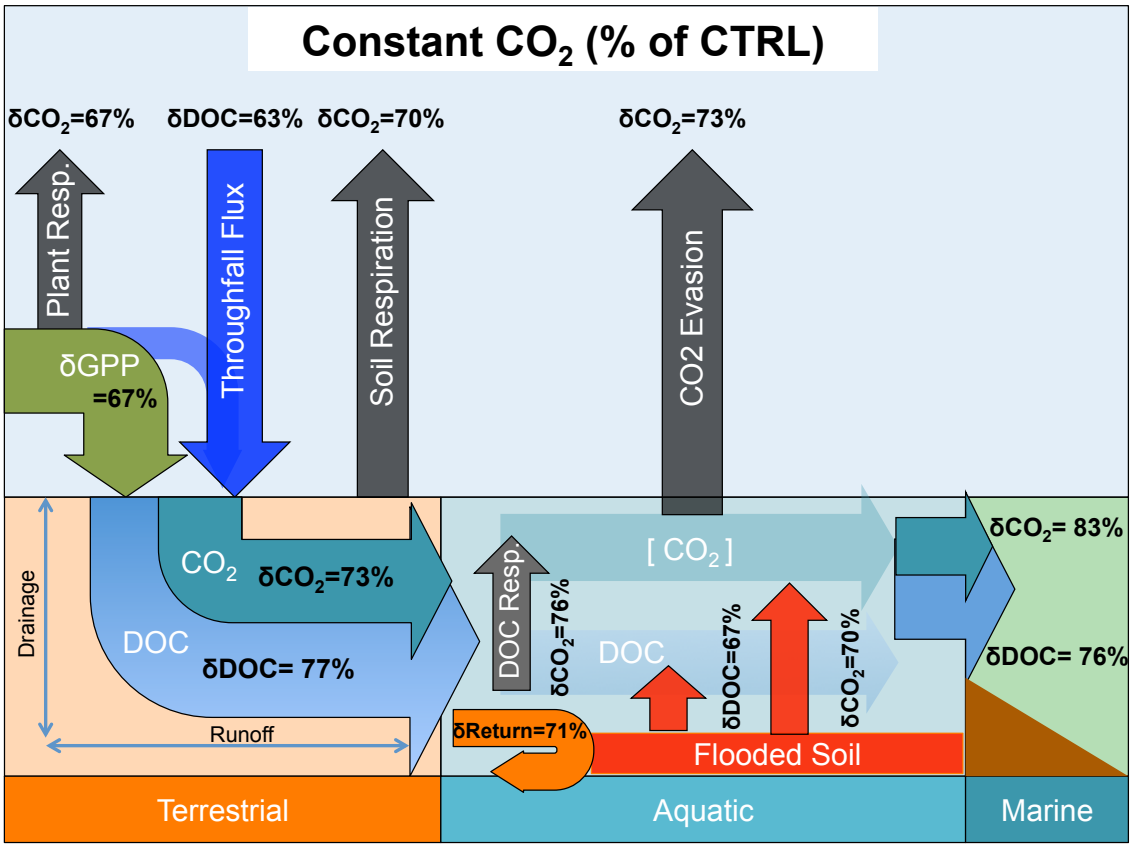

Figure 12: **(a)** Simplified 'leaky pipe' diagram representing the transport and processing of DOC within the land-ocean hydrologic continuum. The scheme template is taken from Cole et al. (2007), where we reproduce their global estimate of DOC and non-groundwater discharge portion of this flow in the top panel (PgC yr^{-1}), and the equivalent flows from our Lena basin simulations in TgC yr^{-1} in the bottom panel. Thus easy comparison would look at the relative fluxes within each system and compare them to the other. **(b-c)**: Schematic diagrams detailing the major yearly carbon flux outputs from simulations averaged over the period 1998-2007 as they are transformed and transported across the land-aquatic continuum. Figures **(b)** and **(c)** give the same fluxes as a percentage difference from the Control (CTRL-Simulation), for the constant climate and CO_2 simulations, respectively.

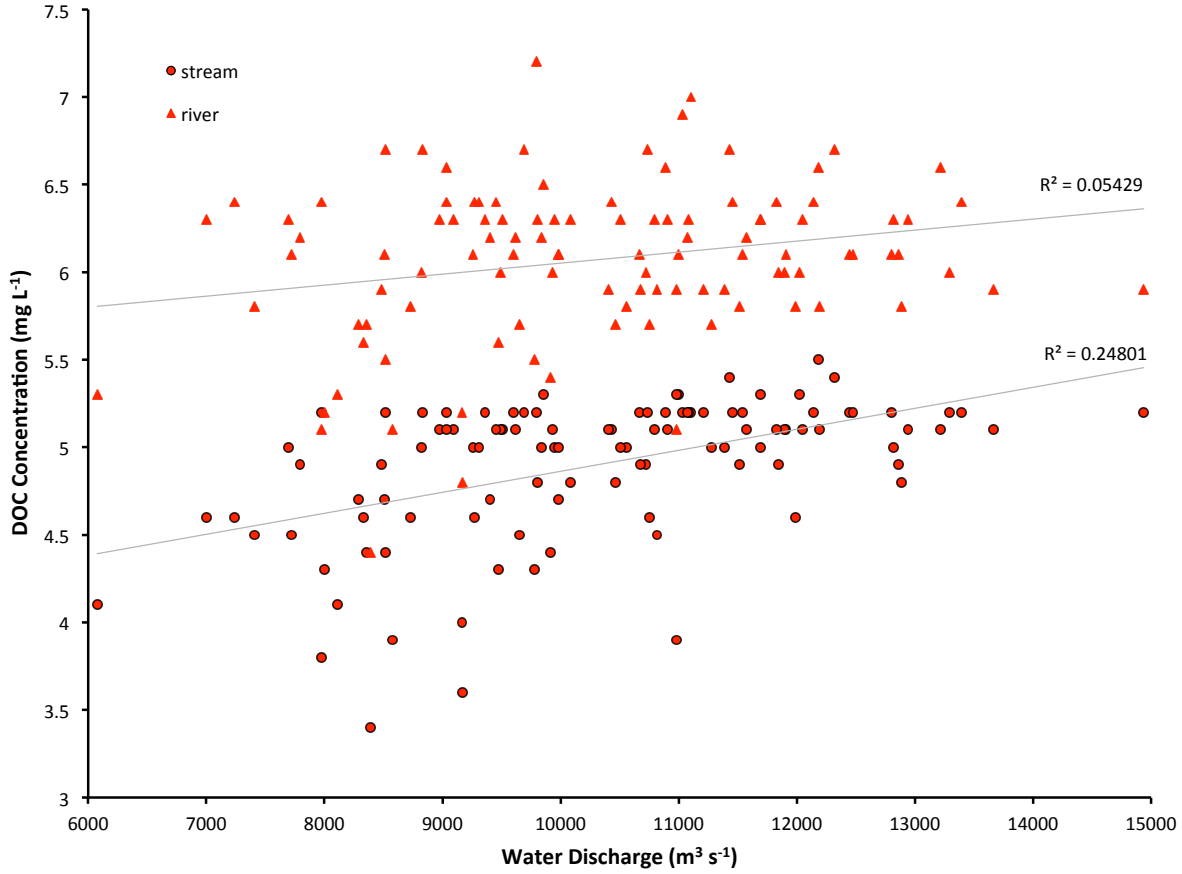

Figure 13: Simulated basin-mean annual DOC concentrations (mg L^{-1}) for the stream and river water pools regressed against mean annual simulated discharge rates (m^3 s^{-1}) at Kusur over 1901-2007. Linear regression plots with corresponding R^2 values are shown.